The copyright of this thesis vests in the author. No quotation from it or information derived from it is to be published without full acknowledgement of the source. The thesis is to be used for private study or non-commercial research purposes only.

Published by the University of Cape Town (UCT) in terms of the non-exclusive license granted to UCT by the author.

University of Cape Town

THE EROSION OF WC-Co COATINGS

BY

SIPHILISIWE NOMPUMELELO NDLOVU

University of Cape Town

Thesis submitted to the Faculty of Engineering and the Built Environment of the University of Cape Town in fulfillment of the requirements for the degree of Master of Applied Science.

Centre for Materials Engineering

Department of Mechanical Engineering

University of Cape Town

August 2002

ACKNOWLEDGEMENTS

I would like to thank the following people for their support during the time this work was carried out:

Professor Colin Allen, my supervisor, for his guidance and constant encouragement.
Mr. Hugo Howse, from CSIR for supplying the materials and for his advice and enthusiasm.
Professor H-G. Sockel from Erlangen University for my time spent studying and travelling in Germany.
Mr. Glen Newins and Mr. Peter Jacobs for their endless workshop assistance and machine repairs.
Mrs. Heidi Lovelock for her assistance with the project.
Dr. Mira Topic for her laboratory assistance and advice.
Mrs. Miranda Waldron of the Electron Microscope Unit (U.C.T.) for her patience, advice and assistance with microscopy.
Mr. Maitse Sello, for assistance with calibrating the slurry rig and formatting of this document.
Mr. Craig Pike for carrying out the corrosion tests.
Mrs. Norma Africa for all her administrative assistance
Mrs. Doreen Young, for providing a clean working environment.
My friends and colleagues in the Centre for Materials Engineering, for their support and much needed humour.
Mr. Siyabonga Mapoko and Miss Tebogo Mabotha for proof reading this thesis.
My family for their belief in me and constant encouragement.
The financial support of the Centre for Materials Engineering and the National Research Foundation is gratefully acknowledged.

Dedicated to my beautiful niece, Hlengiwe Ndlovu, born on 2 February 2002.

University of Cape Town

ABSTRACT

A study has been conducted on both the particle and slurry erosive wear behaviour of WC-Co hard metal coatings. The coating compositions were WC-12%Co and WC-10%Co-4%Cr and were produced using both the TAFA JP5000 and the METCO Diamond Jet (DJ) thermal spray systems. Particle erosion testing was carried out on an air blast apparatus using silica with a size range of 75-150μm at a velocity of 66ms^{-1}. Slurry erosion was conducted with the same erodent at a concentration of 11wt% in a water stream flowing at 7ms^{-1}.

The results have shown that the coatings produced by the different methods have similar structures and properties and respond in a similar manner in the different tests. The coatings had a better wear resistance than a sintered WC-10%Co material. It has been shown that the chromium containing coatings have a superior resistance to both particle and slurry erosion, particularly slurry erosion, compared to the WC-Co coatings. This has been attributed to the change in the matrix properties and corrosion resistance of these coatings.

University of Cape Town

CONTENTS

University of Cape Town

University of Cape Town

University of Cape Town

University of Cape Town

CHAPTER 1

INTRODUCTION

1.1 INTRODUCTION TO WEAR

Wear is defined as the progressive loss of material from the surface of a solid body due to mechanical action, i.e. the contact and relative motion of a body against a solid, liquid or gaseous counterbody [1]. Wear occurs in many different situations, for example, in piston rings, gears and in human body joints such as the knee and hip. In all these cases widely varying wear conditions exist. Friction and wear are both characteristics of the engineering system, which is called the tribosystem; represented in Figure 1.1.

The tribosystem in most cases consists of four elements,

1. A solid body,
2. Counterbody,
3. Interfacial element,
4. Environment.

The nature of the various elements that make up the tribosystem will clearly have a direct effect on the wear process. The counterbody may be a solid, a liquid, a gas or a mixture of these. Interfacial elements include lubricants, adsorbed and oxidised layers and solid particles.

University of Cape Town

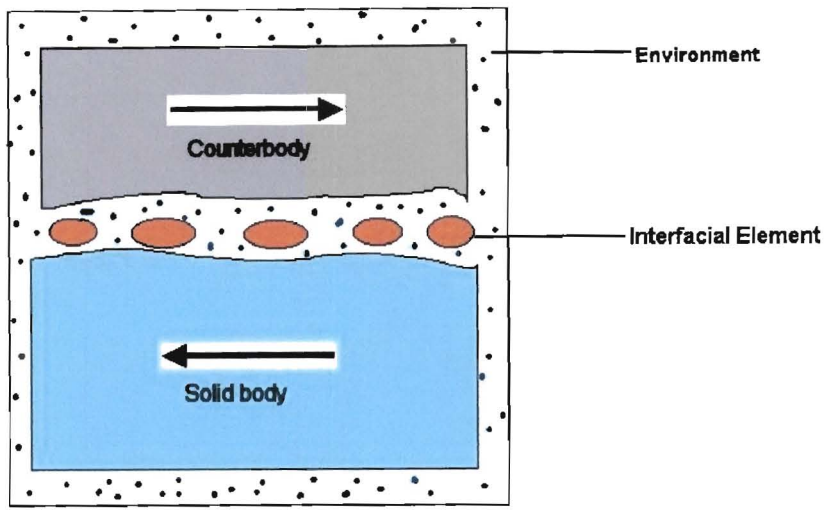

Figure 1.1: Schematic of the elements in a tribosystem [1]

The material's intrinsic surface properties such as hardness, strength and ductility are also important factors that affect the wear resistance of a component. In addition to the material properties other factors such as the surface finish, load, speed, corrosion, temperature and properties of the counterbody also play an important role in the wear process.

The mechanism of wear is very complicated and the theoretical treatment of wear usually simplifies the processes that take place into three broad categories. These are abrasion, adhesion and erosion, which may act individually or in combination.

University of Cape Town

1.2 Abrasive Wear

In abrasive wear, material is removed or displaced from a surface by hard particles, or by hard protuberances on a counterface, forced against and sliding along the surface.

Abrasive wear can be sub-divided into two types: two-body and three body abrasive wear. Two-body abrasive wear is caused by hard protuberances on the counterface, while in three-body abrasive wear hard particles are free to roll and

slide between two surfaces. Two-body wear is normally more severe than three-body abrasion and may be one degree of magnitude greater [2,3,4]. This is because loose abrasive particles only abrade the surface 10% of the time and spend 90% of the time rolling [5].

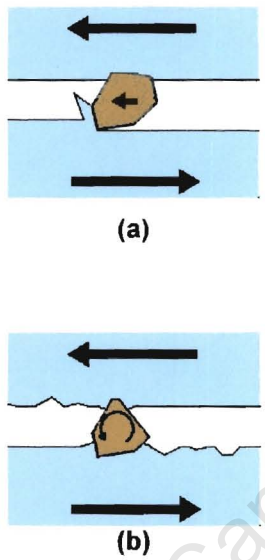

Figure 1.2: Illustration of the differences between (a) two-body abrasion and (b) three-body abrasion

Material loss in abrasive wear occurs generally through two processes namely, ploughing and cutting. In ploughing, an abrasive particle pushes material in its path to both sides of the wear groove. Volume loss due to the single passage of an abrasive particle does not occur but the repeated action of many abrasive particles leads to the eventual removal of material as the result of low cyclic fatigue [1].

University of Cape Town

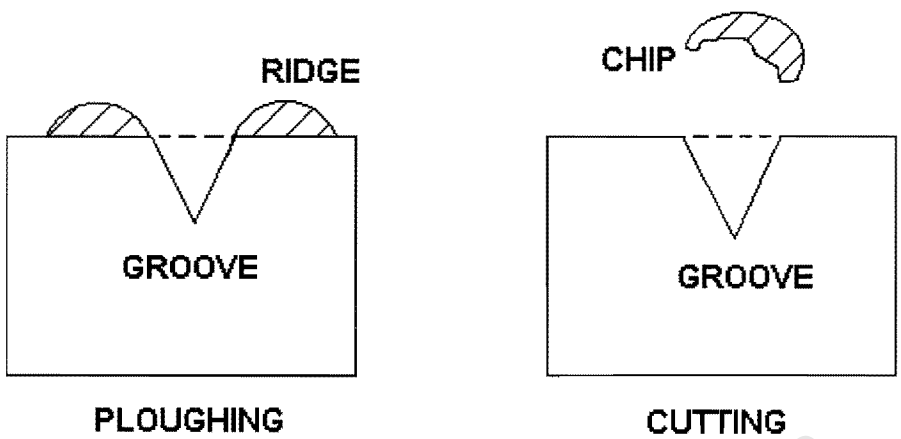

Figure 1.3: Schematic showing the two mechanisms of abrasive wear in materials

University of Cape Town

Cutting leads to the removal of material from the surface by the formation of chips, shavings and fragments. The surface is worn and a groove is formed whose geometry depends on the size and shape of the abrasive particle. Cutting causes the most severe rate of abrasive wear in ductile materials [6].

1.3 Adhesive Wear

Adhesion is the formation and breaking of interfacial adhesive bonds e.g. cold-welded junctions. This can take place when surfaces slide against each other. Sliding leads to high local pressure between contacting asperities, which results in plastic deformation, adhesion and the consequent formation of junctions locally. Relative sliding between the contacting surfaces leads to the rupture of these junctions and subsequent material transfer from one surface to the other, in addition to the production of debris and material loss. The presence of a lubricating or oxide film reduces the tendency for adhesion to occur [6].

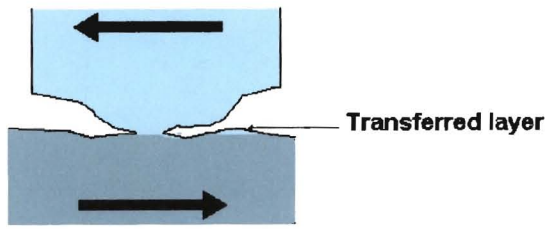

Figure 1.4: Schematic of adhesive wear

1.4 EROSIVE WEAR

Erosion is caused by a gas or a liquid which may (or may not) contain solid particles, impinging on a surface. The impact of a particle against the target surface produces a local damage event, which leads to the removal of material by various mechanisms.

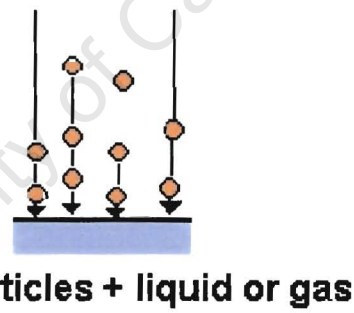

University of Cape Town

Figure 1.5: Schematic of the erosive wear process

Erosion is generally divided into several forms depending on the elements that are interacting in the particular system. These are commonly called particle, slurry and cavitation erosion.

1.4.1 SOLID PARTICLE EROSION

Solid particle erosion occurs in many applications when solid particles entrained in a fluid stream strike a surface resulting in the displacement or removal of material. The response of a material to erosive wear by solid particles is influenced by the properties of the material such as the hardness and microstructure, the fluid flow conditions, i.e. the number of particles striking the surface, the direction and the velocity of the particles. Furthermore, the properties of the abrasive particles also affect the amount and mechanism of material loss that occurs.

1.4.2 SLURRY EROSION

Slurry erosion refers to a situation in which the material is exposed to impinging particles in a corrosive liquid environment. Slurry erosion is important in many industrial applications such as slurry pumps in mining and in the production of natural gas. The material's response depends on its resistance to the erosive particles in the slurry, its corrosion properties and its response to the combined effect of these two degradation mechanisms.

1.4.3 CAVITATION EROSION

Cavitation is the formation and collapse, within a liquid, of cavities or bubbles that contain vapour or gas. This usually originates from changes in pressure in the liquid brought about by turbulent flow or by vibration, but can also occur from changes in temperature. Cavitation erosion occurs when bubbles or cavities collapse on or very near the eroded surface. The mechanical shock induced by cavitation is similar to that of liquid impingement erosion causing direct localised damage of the surface or by inducing fatigue.

University of Cape Town

1.5 Aims And Objectives Of The Present Work

The methods employed to combat wear vary widely due to the systems dependency of the total process. Surface engineering, such as the use of hard coatings is favoured in many cases since they can be applied to components of all shapes and sizes. Consequently, high velocity oxy-fuel sprayed WC-Co coatings are used in a wide variety of situations such as boiler tubes, pumps and valves to reduce wear.

However limited quantitative information is available on the relative merits of different hard metal coatings in erosive wear, particularly subjected to slurry erosion. This work is an attempt to assess the wear performance of oxy-fuel sprayed WC-12%Co and WC-10%Co-4%Cr coatings subjected to both particle and slurry erosion.

The specific objectives of the work were to:

1. Characterise the feedstock powders and structures of the hard metal coatings produced by the TAFA JP5000 and Sulzer Diamond Jet HVOF spray systems.
2. Determine the wear rates of WC-12Co and WC-10Co-4Cr coatings subjected to both particle and slurry erosion using silica.
3. Analyse the mechanisms and modes of wear that predominate under both conditions
4. Correlate the wear performance with microstructural and property parameters.
5. Compare the performance of coatings applied by the two different spray methods, namely the TAFA JP5000 and Diamond Jet spray systems.

University of Cape Town

CHAPTER 2

LITERATURE REVIEW

EROSIVE WEAR

2.1 INTRODUCTION

Wear is not often catastrophic but may lead to increased clearances between moving components, unwanted freedom of movement, increased vibration and mechanical loading which in turn accelerates the wear process. The loss of relatively small amounts of material as a result of erosion can be small enough to cause complete failure of large complex systems in cases where fine tolerances are essential for the successful operation of the machinery [7].

Wear as stated earlier is not an intrinsic material property but a characteristic of the engineering system. The wear rate depends on a large number of parameters in the tribosystem which all interact with each other.

The objectives of this chapter are to firstly describe more fully the different erosive wear processes that can occur and to discuss the mechanisms of material loss.

University of Cape Town

2.2 GENERAL MATERIAL RESPONSE TO EROSION

The mode of material removal during erosive wear is determined primarily by the properties of the target material.

2.2.1 BRITTLE WEAR MECHANISMS

Erosion in brittle materials occurs by the formation and interaction of subsurface cracks. The surface stress must reach a critical value to initiate microcracking, followed by crack propagation and the intersection of these cracks, which leads to the eventual loss of material [8].

The erodent particle velocity, shape and mechanical properties of the target material determine the deformation and fracture modes. Blunt particles travelling at low velocities set up Hertzian stresses which leads to cone cracking, Fig. 2.1. Sharp particles travelling at high velocities cause inelastic deformation which initiates median and lateral cracking, Fig 2.2.

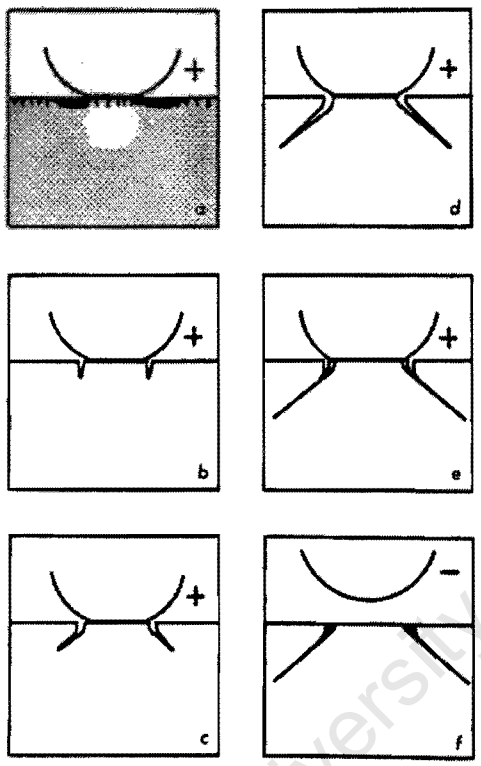

Figure 2.1: Sequence of events during cone-cracking. Cracks form during the loading cycle and deviate outwards in order to avoid the compressive zone immediately beneath the indenter (this zone is indicated by the white region) [9]

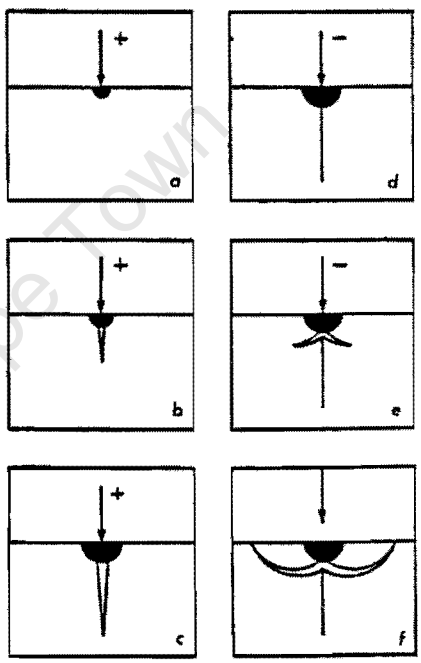

Figure 2.2: Sequence of events during lateral cracking. Median cracks form during the loading cycle due to the high stress concentration immediately beneath the indenter . Lateral cracks form during the unloading cycle, due to the tensile stresses imposed by the pressure of the deformed material (this zone is indicated by the dark region) [10]

University of Cape Town

2.2.2 DUCTILE WEAR MECHANISMS

Ductile materials erode through a combination of microcutting and ploughing, microcutting is dominant during high angle erosion and microploughing is dominant during low angle erosion.

Microcutting normally occurs when hard angular particles impact the surface and material is gouged from the surface [8]. Ploughing leads to the formation of extruded lips on the perimeter of the crater and eventual material loss ocurs as the result of subsequent particle impacts, Fig. 2.3.

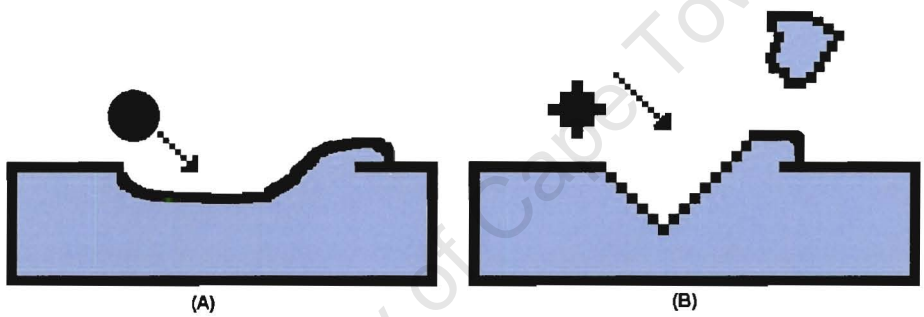

Figure 2.3: The mechanisms of material removal by hard particles on a ductile material (a) Ploughing deformation with a sphere and (b) Cutting deformation with an angular particle

University of Cape Town

The most efficient material removal mechanisms are considered to be microcutting in ductile materials and lateral cracking in brittle materials.

2.3 VARIABLES AFFECTING EROSION

The erosion response of a material is determined by its mechanical and microstructural characteristics and by the parameters of the erosive system. The important variables are summarised in Figure 2.4.

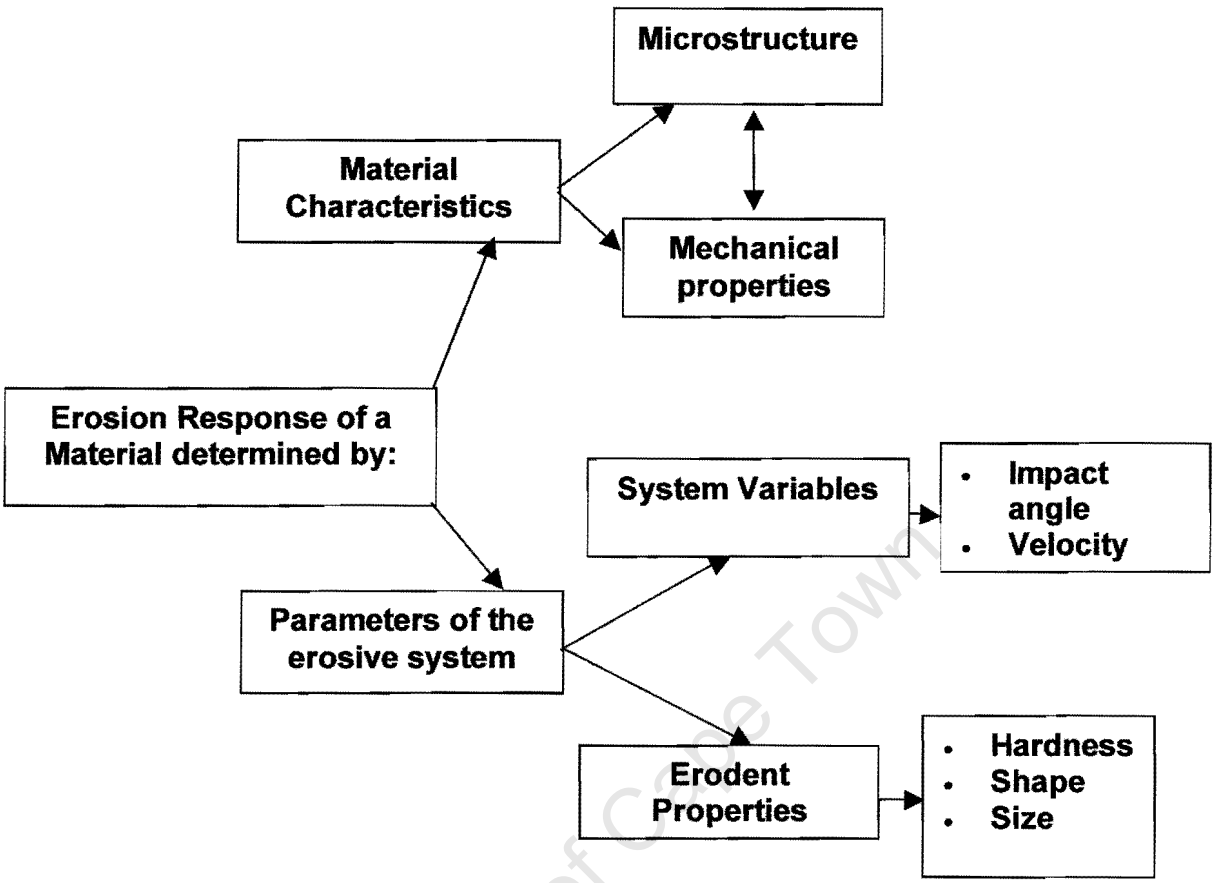

Figure 2.4: Flow chart showing the parameters which influence the erosion response of a material

University of Cape Town

2.3.1 TARGET MATERIAL PROPERTIES

HARDNESS

Hardness is the measure of a material's resistance to plastic flow. Finnie et al found the erosion rate to decrease with the reciprocal of hardness for different materials [11]. However, little change was observed when the hardness of an individual alloy was varied through different thermal treatments or by work hardening. Levy found the erosion rate to vary inversely with hardness for a 1075 steel and two harder 1020 steel samples [12]. However, other researchers have found there to be no significant change in the erosion rate with an increase in hardness [13, 14, 15]. For example, work by Brass indicated that the erosion rate of an aluminium copper alloy and a carbon steel did not correlate with

hardness measurements and only a slight variation was observed, despite major microstructural changes induced by thermal treatment [16].

Srinivasan and Scattergood determined that the relative hardness values of the erodent particles and the target sample play an important role during erosion [17]. Mechanisms that involve lateral crack growth operate for harder erodents but in the case of softer erodents damage accumulation is required to build up adequate stresses to produce lateral cracking. A significant increase in the erosion rate is observed when the erodent particle-to-target ratio H_E/H_T increases above 1. Vaughan and Ball also found the ease with which lateral cracks initiate to be a controlling factor in the erosion of ceramics and ultra hard materials when the erodent particles and target material were of similar hardness [18].

Generally, it is expected that increasing the hardness of a material increases its erosive wear resistance. However many exceptions to this trend exist and hardness is a poor predictor of a material's response to erosion.

University of Cape Town

FRACTURE TOUGHNESS

Fracture toughness is a measure of a material's resistance to fracture propagation. In brittle materials, crack initiation and growth leads to the eventual loss of material, therefore increasing K_{IC}, the fracture toughness of the material should improve the wear resistance of the material. Sykes et al found this to be true as they found the erosion resistance of an Al_2O_3-SiC composite to increase with additions of up to 25wt% SiC which raised the fracture toughness of the material [19]. However work by Morrison, Routbort and Scattergood showed the erosion behaviour of Si_3N_4 material to be independent of the fracture toughness of the material as the erosion resistance did not change when the whisker content was increased by the addition of SiC which increased the material's toughness [20].

The erosion behaviour of a plain carbon steel, an austenitic stainless steel and a low alloy steel in various heat treated conditions was investigated by Foley and

Levy [21]. The tests were conducted using 140μm alumina particles and it was found that the fracture toughness and impact strength of the materials had little effect on their erosion behaviour.

MICROSTRUCTURE

The microstructure has an influence on the hardness and strength of the material and hence affects the wear mechanisms that occur during impact of particles on the material surface. Microstructural defects may also act as crack initiation sites or may even cause crack arrest [22]. For example, porosity affects the erosion rate of a material as it inhibits crack propagation by blunting crack tips [23]. Furthermore, lateral crack growth can be inhibited by grain boundaries which effectively reduces the size of the damage zone and reduces the erosion rate.

In MgO, cracking along grain boundaries occurred close to the impact zone leaving loosely bound grains which were consequently easily removed by further impacts. Therefore the grain size is very important in this particular material [23].

2.3.2 ERODENT PROPERTIES

HARDNESS

Soft erodent particles tend to blunt on impact therefore reducing the likelihood of lateral crack initiation and favouring Hertzian cracking of brittle materials. Harder particles are better able to retain their shape and hence more able to concentrate their energy on the target surface. Work by Wada et al. and Head et al. showed that the properties of the erodent particles affect the erosion rates and the crack morphologies of brittle materials [24, 25]. An increase in erosion rate with increasing erodent particle hardness was observed. On the other hand, Evans et al. observed little change in the wear rate with increasing erodent particle hardness at a 90° impact angle [26].

University of Cape Town

Levy and Chik found that above a particle hardness of 700HV, the erosion rate of mild steel is essentially independent of the hardness-strength characteristics of the erodent [12].

SHAPE

In general, spherical particles cause a lower wear loss than angular particles at a given average particle size [21, 27]. Angular particles remove material more efficiently by microcutting and lateral cracking leading to higher wear rates. According to Wiederhorn et al. sharp particles have greater ability to concentrate stresses and induce irreversible deformation which leads to lateral cracking [28]. Work by Sparks and Hutchings focused on the effect of impact velocity, angle and particle shape on the erosion of silicate glass-ceramic [29]. They observed the variation of the erosion rate with impact velocity for two types of silica particles at an impingement angle of 30°. A sharp increase in erosion rate at velocities between 44 and 52ms^{-1} was observed for the rounded particles whereas with the angular particles a constant velocity exponent applied. Above a particle velocity of 52ms^{-1}, the erosion rate due to angular silica particles was approximately 1.5 times that measured with the rounded particles. Below this velocity, which was considered to be the transition point, the erosion due to angular particles was 10 times greater than with rounded particles. Above the transition point, material removal was in the form of large flaky fragments formed by lateral fracture. Below the transition point, material removal by the rounded particles involved less fracture.

Winter and Hutchings studied the effect of particle shape on wear rate in ductile materials [30]. The particle shape determines the rake angle which was defined as the angle between the front face of the particle and the normal to the target surface. Spherical particles are associated with large and negative rake angles. Ploughing occurs for large rake angles and cutting takes place with small rake angles. Angular particles are found to cause a greater amount of material loss via a cutting mechanism.

University of Cape Town

SIZE

In the case of ductile materials, various studies carried out between 1970 and 1981 and more recently in 1989 have shown that the erosion rate increases for increasing particle size up to a diameter of about 100μm [31, 32, 33, 34]. Above this critical value the erosion rate is independent of particle size. Goodwin et al found the critical size to increase linearly with velocity when they studied the influence of particle size and velocity on an 11% chromium steel.

The size effect was explained by Misra and Finnie who concluded that it is due to shallow surface layers which work harden more than the bulk material when they are eroded or abraded [31]. A hardness gradient is formed by the impact of particles, small particles are unable to penetrate this layer thereby removing less material. However, sufficiently large particles are able to penetrate the hard layer and will therefore cause plastic deformation of the material. Therefore, after some critical size, the influence of the hard layer becomes insignificant. It has however been shown that heat treatment of the bulk material to a range of hardness and various degrees of cold work have no effect on the erosive wear of the material [35].

For brittle materials, the relationship between erosion rate and particle size is not so clear. Some work concludes that the erosion rate is an exponential function of the particle size which varies according to the shape of the component or specimen being eroded [36, 37]. However in some brittle materials a critical particle size similar to that in ductile materials has been observed [38].

The size range of the erodent particles also affects the erosion rate, a wide size distribution usually leads to a higher erosion rate. Marshall et al. found that the erosion rate increased as the particle size range of the erodent was expanded [39].

University of Cape Town

2.3.3 SYSTEM VARIABLES

IMPACT ANGLE

Ductile materials exhibit a maximum erosion rate at low impact angles between 20° and 30°. These conditions result in material removal by ploughing and microcutting. In brittle materials the maximum erosion is exhibited at normal angles of incidence which result in the most severe cracking [13].

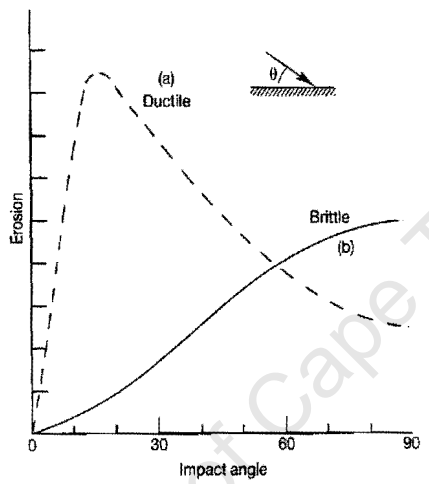

Figure 2.5: The typical dependence of erosion on impact angle

ERODENT PARTICLE VELOCITY

The erosion rate (E_R) varies exponentially with the velocity (V) of the eroding particles for both ductile and brittle materials and the relationship is often expressed in the form:

$$E_R = \text{const } V^n \qquad \text{(Equation 2.1)}$$

In the case of ductile materials the exponent (n) normally lies in the range 2-3. Brittle materials have higher exponent values and these vary widely, exponents of between 1.7 and 7.0 have been reported. Finnie, Wolak and Kabil eroded a range of metals with SiC particles at an angle of 20° and found the velocity exponent ranged from 2.05 to 2.44 [13]. In their studies on glass impacted with steel spheres the exponent value was 6. Bujis et al. reported an exponent of 2.33

University of Cape Town

for glass eroded by alumina particles [40]. Gulden studied the erosion of a series of ceramics including hot-pressed silicon nitride (Si_3N_4), reaction bonded silicon nitride (Si_3N_4), a glass-bonded aluminium oxide and hot-pressed magnesium flouride (MgF_2). She reported that the exponent ranged from 1 to 4 [41]. The reasons for the wide variation observed in the exponent value for brittle materials is unclear.

2.4 SUMMARY

It is absolutely clear from literature that many factors affect the erosion behaviour of solids and great care has to be taken in the interpretation of the results. The effects of the various parameters to be considered are summarized below.

Target material properties

Hardness: It is generally expected that an increase in the material's hardness increases its wear resistance, but this is not always the case, making hardness a poor indicator of a material's response to erosion.

Fracture toughness: An increase in the fracture toughness generally leads to an increase in the wear resistance, but in some cases it has been shown to have no effect on the wear rate.

Micostructure: The microstructure affects the hardness and strength of a material and therefore influences the wear resistance of the material. The presence of defects is usually detrimental but in some cases defects such as pores may inhibit crack growth, thereby improving the wear performance of the material.

Erodent properties

Hardness: Generally increasing the erodent hardness increases wear rate and the erosion rate is also affected by the ratio of the target hardness to the erodent hardness.

University of Cape Town

Shape: Angular particles cause more efficient material removal, subsequently producing higher wear rates than spherical particles

Size: For brittle materials there is no clear relationship and in the case of ductile materials there is a threshold size above which increasing erodent particle size has no effect

System variables

Impact angle: Ductile materials exhibit a maximum erosion rate between 20° and 30° whereas brittle materials exhibit a maximum wear rate at 90°.

Erodent particle velocity: The erosion rate varies exponentially with particle velocity (Equation 2.1). The exponent is between 2 and 3 for ductile materials but in the case of brittle materials the exponent value varies widely.

University of Cape Town

CHAPTER 3

LITERATURE REVIEW

WC-Co ALLOYS

3.1 INTRODUCTION

Cemented tungsten carbide is commercially one of the oldest and most successful powder metallurgy products [42]. These carbides are made by "cementing" very hard tungsten monocarbide grains (WC) in a binder matrix of tough cobalt metal (Co) by liquid phase sintering. The high solubility of WC in cobalt at high temperatures and the excellent wetting of WC by the liquid cobalt binder result in optimum densification during liquid phase sintering producing a structure with little porosity [43]. As a result, the cemented carbide has high strength, toughness and hardness.

The unique composite structure of hard WC grains in a tough cobalt matrix results in excellent wear resistance. As a result, cemented carbides find extensive use in a variety of structural components, in which wear is important such as sand blast/spray nozzles, seals in slurry pumps and component parts in the oil industry [44, 45].

University of Cape Town

The objective of this section is to describe the influence of microstructure on the wear of WC-Co alloys with emphasis on the wear mechanisms during erosion that have been observed.

3.2 THE CONSTITUENT PHASES

3.2.2 COBALT

Cobalt is the most commonly used binder for WC because of its excellent carbide wetting and adhesion properties. The capillary action of cobalt during sintering allows the achievement of high densities.

Cobalt exists in two allotropic forms, the hexagonally close packed (h.c.p.) form which is stable at temperatures below 417°C and the face centered cubic (f.c.c.) form which is stable up to a temperature of 1495°C; the melting point of cobalt [46, 47]. However, a significant amount of f.c.c. Co is present in sintered WC-Co hardmetals at room temperature.

3.2.2 TUNGSTEN CARBIDE

Tungsten combines with carbon to form two carbides, WC which has a microhardness of 2400kg/mm^2 and W_2C with a microhardnesses of 3000kg/mm^2 [48]. Pure WC does not melt under standard atmospheric conditions, but decomposes into a liquid phase and graphite above a temperature of approximately 2780°C as seen in the W-C phase diagram (Figure 3.1). The wettabilty of WC by most binder metals is good, making it the popular carbide choice for sintered hard metals.

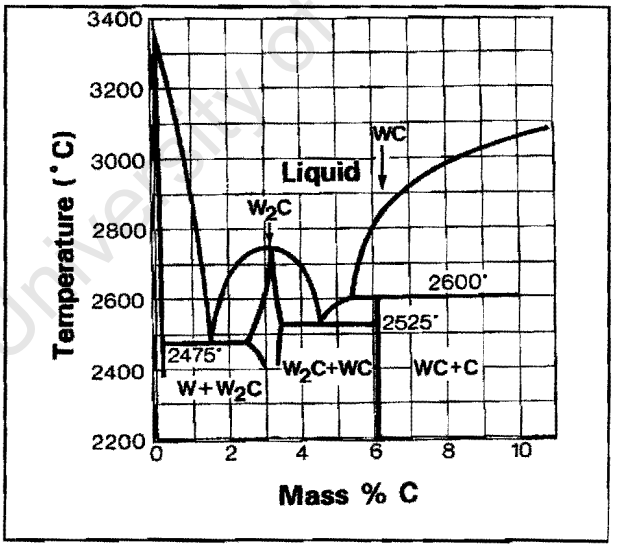

Figure 3.1: Simplified equilibrium phase diagram for the binary system W-C [49].

The major phase in cemented carbides is the monocarbide, WC. This has a simple hexagonal crystal structure with two atoms per unit cell and a c/a ratio of

University of Cape Town

0.976 [46]. This is the only binary phase present at room temperature and it has almost no solid solubility up to 2384°C.

3.3 Microstructural Features Of WC-Co Alloys

The grain size of the WC powder used, the amount of cobalt added and the processing parameters such as the sintering time and temperature determine the microstructure of the cemented carbide [50]. The four features that characterize the microstructure are the WC grain size, cobalt content, binder mean free path and contiguity. There is also some inherent porosity as a result of the processing route used in the manufacture of the material.

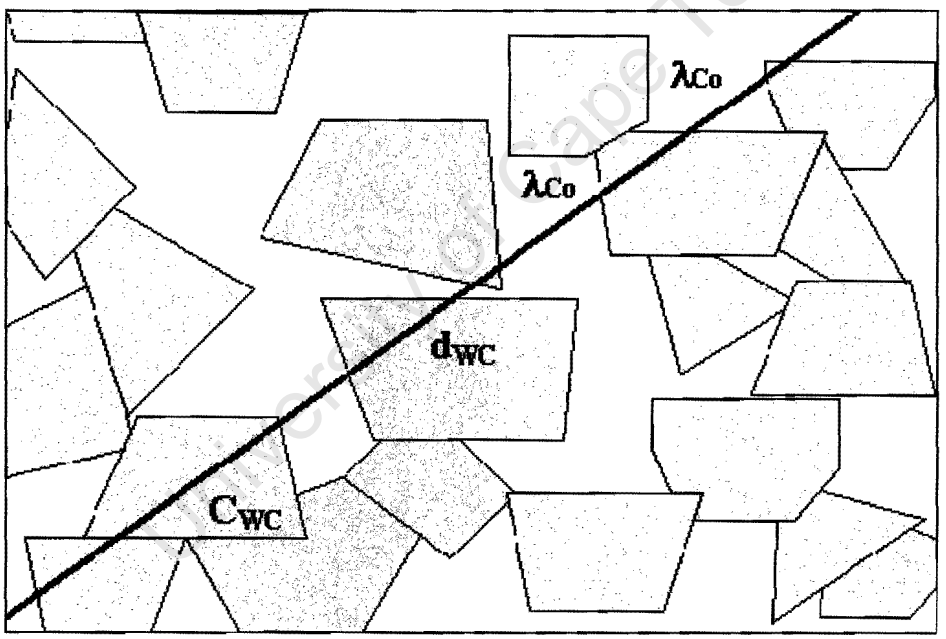

University of Cape Town

Figure 3.2: A schematic representation of the WC-Co alloy illustrating the microstructural parameters, where λ_{Co} is the mean free path of the binder phase, d_{WC} is the WC grain size and C_{WC} is contiguity

3.3.1 WC Grain Size

The WC grain size is defined as the mean linear intercept of the WC phase. The WC grain size influences the fracture properties of the material since the strength

of individual carbide particles decreases with increasing size [51]. Work by Exner illustrated how the hardness and compressive strength decreases with increasing WC grain size [52].

The transverse rupture strength showed a maximum at a WC grain size of approximately 3μm for the WC-12%Co alloy studied, which has been explained in terms of crack propagation. Fracture takes place mainly in the cobalt phase in alloys with a small carbide size, but in coarse alloys proceeds preferentially through the WC grains. The maximum strength of the material is realised when both phases have equal strength.

3.3.2 Cobalt Content

Cemented carbides used in technical applications normally contain between 5 to 25wt% cobalt. The hardness of the material decreases with increasing cobalt content while the compressive strength reaches a maximum at 5wt% Co and then drops sharply when the cobalt content is increased [53, 54]. The transverse rupture strength on the other hand improves with increasing cobalt content up to a maximum at a cobalt content of approximately 20wt%. The reported results are for an alloy with a medium WC grain size of 2μm. The composition that provides maximum strength depends on other variables such as the WC grain size [55, 56, 57]. In some cases a maximum strength has been observed with a cobalt content greater than 30wt%.

3.3.3 Binder Mean Free Path

The mean free path (λ) is defined as the average thickness of the binder between the WC grains and is dependent on the cobalt content and the size of the WC grains.

The transverse rupture strength exhibits a maximum when plotted against the binder mean free path [52]. The hardness and compressive strength decrease with increasing binder mean free path.

University of Cape Town

3.3.4 CONTIGUITY

Contiguity is a measure of the continuity of the carbide skeleton existing within a WC-Co alloy and is defined as the fraction of the total WC grain boundary surface area that is taken up by the WC/WC interface [52]. Contiguity decreases with increasing binder content, decreasing WC grain size and is also dependent on the processing history of the carbide [58].

It is difficult to determine the effect of contiguity on the mechanical properties due to other microstructural characteristics that must be taken into consideration. However, the limited work that has been carried out shows increasing hardness and decreasing rupture strength with increasing contiguity [52, 59]. This relationship is demonstrated in Gurland 's work. He observed a sharp decline in the rupture strength from approximately 300 to 130kp/mm^2 when the contiguity was increased from 0.55 to 0.65 [52].

University of Cape Town

3.4 EROSION OF WC-CO ALLOYS

3.4.1 INTRODUCTION

The dominant mechanism of wear is dependent on the microstructure of the cemented carbide and the scale of individual particle contacts. In the case where the erosive particles are small enough to penetrate between the WC grains, wear can occur by the preferential erosion of the metallic binder phase. This leads to undercutting and the eventual loss of whole carbide grains. If the binder regions are too small to allow penetration by the erosive particles this results in erosion of the carbide and the binder. With large erodent particles, fracture of the WC grains becomes important. The combination of these mechanisms leads to a dependence of the erosion rate on the binder content and WC grain size [60].

3.4.2 EROSIVE WEAR MECHANISMS

Anand and Conrad proposed that particle erosive wear mechanisms of cemented carbides depend on the size of the impact damage in relation to the microstructure [60]. Small impacts involving less than 10 WC grains lead to a

brittle erosive mode and for impacts involving more than 100 WC grains, a ductile wear mode takes place.

Crushing and cracking of WC grains occurs during brittle behaviour, the appearance of the cracks being different from those normally associated with lateral and cone cracking. In the ductile regime, WC grains do not undergo any significant deformation and the damage mechanism is ploughing of the binder phase and the subsequent loss of WC grains. The ductile nature of the binder is the controlling parameter, therefore, the erosion rate is very sensitive to the binder mean free path.

3.4.3 Microstructural Effects On Erosion Rate

Cobalt Content

Work by Dankin on a range of cemented carbides with cobalt content ranging from 6-20% yielded a maximum wear rate at an impact angle of 60° and cobalt content of 20% [61] .

Ball and Patterson carried out particle erosion tests on ten different WC-Co materials at an impact angle of 45° and observed a maximum erosion rate at a cobalt content of 10wt% [62].

Erosive wear resistance requires a combination of high hardness and high fracture toughness. In the work done by Dankin this is clearly demonstrated since the hardness of the cemented carbide is inversely proportional to the cobalt content, resulting in a low hardness and poor wear resistance for the 15 and 20wt% material.

Ball and Patterson studied the wear surfaces of the materials to determine the wear mechanisms taking place. They concluded that below 10wt% cobalt content, a process of deformation and fracture of the WC grains took place, while above 10wt% cobalt a more complex mechanism of cutting, ploughing and

University of Cape Town

deformation of the cobalt binder was active. Below 10wt% cobalt the dislocation motion in the binder phase is restricted leading to brittle behaviour even though the material is ductile in nature. Between 10 and 20wt% an increase in the micro toughness of the binder phase as a result of improving dislocation motion is responsible for the increase in wear resistance. However, above 20wt% the effect of decreasing hardness in the alloy led to an increase in the erosion rate.

Pennefather observed a similar relationship (compared to Ball and Patterson) between cobalt content and erosion rate when tests were done at an impact angle of 45° and higher [36]. However, tests done at 30° and below showed only a small increase in erosion with increasing binder phase. The extrusion of cobalt as a result of impact on the WC followed by cracking of the WC grains was observed to occur at a cobalt content below 10wt%. Above 10wt%Co, cutting and ploughing took place.

Ninham and Levy also obtained results similar to those of Ball and Patterson and also found that the volume loss when changing the binder from Co to CoCr was 10-20 times lower [63]. This is due to strengthening of the binder phase through the addition of chromium.

University of Cape Town

MEAN FREE PATH

There is a decrease in hardness and an increase in macro toughness with increasing mean free path. Keshavan and Jee state that the erosion and abrasion rates of WC-Co increase exponentially with an increase in the mean free path [64]. This relationship correlates well with the results of Freinkel and Luyckx [65].

Pugsley investigated the cavitation erosion behaviour of a series of ultrafine and conventional hard metals with cobalt content ranging from 6 to 15wt% [66]. The ultrafine grades had a grain size of 0.49μm and the grain size in the conventinal

grades ranged from 0.8 to 3μm. The dependence of erosion resistance on the binder mean free path that was obtained from the results is shown in Figure 3.3. An interesting feature of these results is the anomalous behaviour of the erosion resistance relative to the binder mean free path. When the binder mean free path is changed by altering the cobalt content while maintainng a constant grain size, the erosion resistance increases with increasing binder mean free path. However, when the binder mean free path is changed by altering the grain size, at a constant cobalt content, the erosion resistance decreases with increasing binder mean free path.

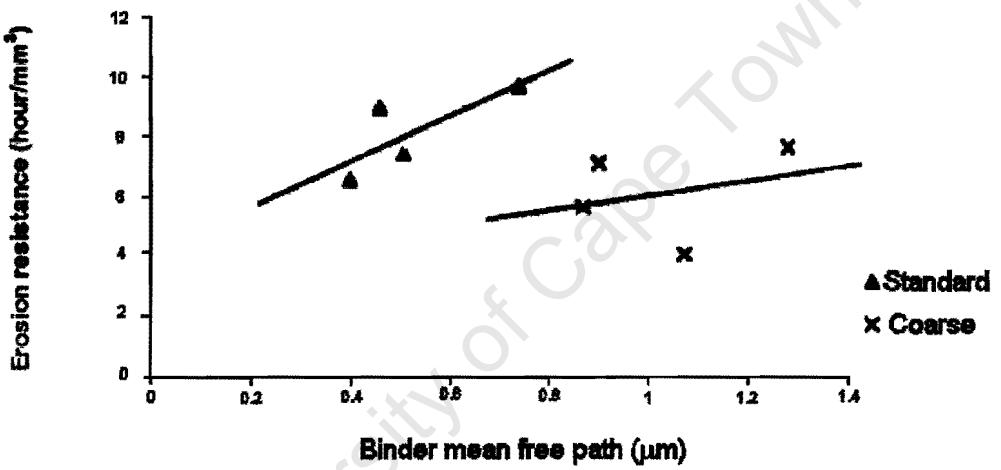

Figure 3.3: Plot of erosion vs binder mean free path for standard and coarse grades [65]

University of Cape Town

WC Grain Size

For a constant cobalt content, the wear resistance has been found to increase with a decrease in WC grain size [67]. Wayne, Baldoni and Buljan observed a slight decrease in the particle erosion rate for 6wt%Co when grain size was reduced but the opposite for the 12wt% material [68].

Work by Freinkel and Luyckx showed that the dependency of wear rate on WC grain size may be a balance between the energy required to erode the cobalt binder phase, the energy absorbed in plastically deforming the WC grains and

the energy lost in plastic deformation and fracture of the erodent [64]. The energy to erode the cobalt decreases with increasing WC grain size and mean free path. A series of WC-Co alloys with grain size ranging from 0.49 to 3μm was studied by Pugsley [69]. A sharp transition in the erosion response of the materials at a WC grain size of approximately 1μm was observed. Below this grain size, the erosion resistance decreases with increasing cobalt content and increases with increasing hardness. Above this grain size however, the erosion resistance increases with increasing cobalt content and exhibits no strong correlation with hardness. This transition is associated with a change in the damage mechanism operating. In sub-micron grades, material removal predominantly occurs in the bulk, leading to the formation of deep erosion craters, which expand laterally eventually coalescing. This produces a steady state erosion surface that is highly undulating and contains small islands of uneroded material. In the standard and coarse grades, material removal occurs mostly on the scale of the microstructure, through the preferential removal of the cobalt phase and the resultant loss of unsupported WC grains.

The observed results were explained in terms of the scaling mechanism proposed by Anand and Conrad [60]. In materials with a fine-scale microstructure, the damage zone caused by particle impact is much larger than the microstructural dimensions and the material responds in bulk to the erosive attack. In materials with a coarser microstructure the scale of the damage zone is comparable to the microstructural dimensions and the constituent phases of the composite respond individually to erosive attack.

University of Cape Town

HARDNESS

There is no defined or clear relationship between hardness and the particle erosion rate for cemented carbides as illustrated by the results of Reshetynak and Kuybarsepp (Figure 3.4) [70]. However for binderless materials, Beste et al found that increasing hardness led to a decrease in the erosion rate [71].

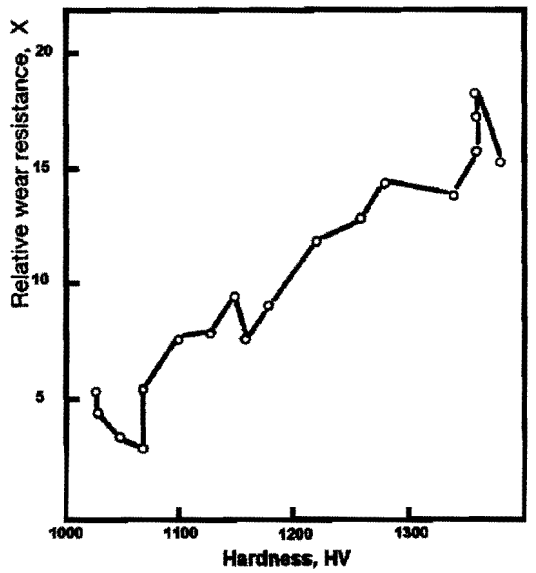

Figure 3.4: Relative wear resistance X versus Vickers hardness number of WC-Co hard metals [70]

When comparing materials with different binder contents the grain size is the more influential factor rather than hardness in predicting the wear resistance.

3.4.4 THE EFFECT OF ERODENT VARIABLES

PARTICLE HARDNESS

Work by Feng indicated a decrease in the particle erosion rate in the order of erodents diamond, SiC, alumina, WC and silica, suggesting that the wear rate increases with increasing hardness of the abrasive particle [72]. Examination of the eroded surfaces also indicated that the mode of surface fracture changed with hardness of the erodent. With increasing hardness of the erodent, the WC-Co surface exhibited increased WC grain fracture which is attributed to a brittle fracture mode.

Softer erodents are likely to undergo plastic deformation during impact reducing the amount of energy available to erode the target material, therefore the erosion rate is lower.

University of Cape Town

The relative hardness of the erodent and target material plays a significant role in the erosion rate. When the erodent and target material are of similar hardness, the ease of fracture initiation and propagation controls the erosion rate and material loss is only possible after repeated impacts. Silica and WC erodents have a lower ability to penetrate the WC-Co surface when compared to the harder diamond and SiC erodents [72, 24].

IMPACT ANGLE

Anand et al. carried out studies on three WC-6%Co materials to investigate the impact angle dependence of particle erosion of these materials [73]. The WC grain size, with a 2μm, 6μm and 16μm in each of the materials tested. There was an increase in wear rate when increasing the WC size and erodent particle size. The majority of the erosion curves showed a peak at an impact angle of 90°, however as the kinetic energy of the erodent particles increased, the erosion curve for the 2μm WC grain size showed a peak at lower angles. As with WC grain size dependence, the results were explained in terms of the size of the impact region.

Freinkel and Luyckx, Dankin and Uuémyis et al all observed a peak in the erosion rate at an impact angle of 60° or lower [64, 61, 67]. When comparing experimental conditions i.e. the erodent size, the mean kinetic energy of the erodent particles the wear mechanism proposed by the theory of Anand was found to hold true.

Pennefather carried out work using similar apparatus to that of Ball and Patterson testing a range of materials at impact angles between 15° and 90° [36, 62]. The WC grain size was between 0.6 and 3.3μm and the erodent velocity used was $40ms^{-1}$. The low cobalt alloys showed brittle behaviour with a maximum wear rate occuring at an incident impact angle. The higher cobalt alloys exhibited a maximum erosion rate at an impact angle of approximately 50°.

University of Cape Town

PARTICLE VELOCITY

Conrad et al. studied the effects of microstructure on the particle erosion of a series of sintered WC-Co alloys [74]. The nominal Co content ranged from 6 to 10.5wt% and the WC grain size was varied from 0.9 to 5.1 μm.

The dependence of erosion rate on velocity was found to obey the power law shown in equation 1, and the values of the exponent are given in Table 3.1.

$$E_R = K v^n \qquad \text{Equation 3.1}$$

where

w is the erosion rate (mass loss per mass of impinged particles)

K is a constant

v is the velocity of erodent particles

n is the velocity exponent (≈2 for WC-6%Co when $\alpha \geq 45°$ and ≈3 when $\alpha = 15°$, similar for higher cobalt content alloys, but n has tendency to increase).

Table 3.1: Particle Velocity Exponent n

Wt%Co	Impingement angle (degrees)		
	90	45	15
6	1.9	1.8	2.7
9	1.9	2.3	3.6
10.5	2.1	2.4	3.6

University of Cape Town

3.5 EROSION CORROSION BEHAVIOUR OF WC-CO ALLOYS

Slurry erosion is a balance between erosion by the solid erodent particles and the corrosion of that material. When corrosion is the dominant process the corrosion resistance of the binder phase becomes very important. When erosion is the controlling factor, the mechanical properties of the cemented carbide have higher importance than the corrosion resistance.

Wright et al. identified four modes of material removal during slurry erosion [75]. These are:

(1) loss of binder

(2) ductile erosion of carbides

(3) brittle erosion of carbides, by chipping and/or fracture

(4) pull out of carbide grains

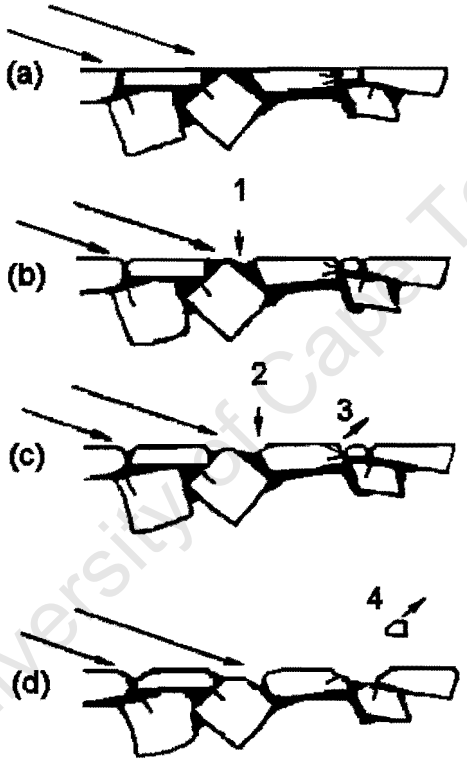

University of Cape Town

Figure 3.5: Schematic representation of Sequences in Slurry Erosion of a WC-Co alloy surface [75]

Pre-existing cracks have been observed in these materials as shown in (a), which represents the as-polished surface. In (b), exposed binder has been removed from between the carbide grains (mode 1). In (c), sufficient binder has been removed leaving corners of the carbide grains exposed and rounding of these occurs by mode 2. Eventual loss of carbide grains is indicated in (d) after sufficient binder has been removed, and the loosely anchored carbide grains fall out (mode 4).

3.5.1 MICROSTUCTURAL FEATURES OF SLURRY EROSION OF WC-CO ALLOYS

Shetty et al. examined the surfaces of a series of sintered WC-Co alloys subjected to slurry erosion [76]. The surface of a 5.1wt%Co alloy was very smooth and even with little evidence of carbide grain pullout. The WC grains had a polished appearance and slightly rounded edges. The cobalt had been removed from the triple-point grain boundary junctions. As the cobalt content was increased the alloys showed increasing evidence of WC grain pullout and the fraction of the surface that was smooth decreased.

3.5.2 MICROSTRUCTURAL EFFECTS ON SLURRY EROSION

EFFECT OF BINDER PHASE

Wentzel and Allen carried out work on several cemented carbides to determine their wear response under corrosive conditions [77]. The work was done on a series of cobalt binder materials and mixed binder materials. The lowest slurry erosion rates occurred when the composition of the binder was mixed, with a high wt% of cobalt and small additions of chromium or chromium and nickel. For all the materials tested, the slurry erosion rates were higher in the salt solution than in tap water. In both salt water and tap water the wear resistance of the 10wt%Co carbide grades was found to decrease when additions of chromium and chromium-nickel were made. An increase in the nickel content of the binder led to an increase in the erosion rate of the material. The nickel had an adverse effect on the material hardness and this was also observed in the 6wt%Co grades. However, in the case of pure nickel there was a decrease in the slurry erosion rate in both fluid mediums. The addition of nickel was found to increase the corrosion resistance of the materials but not the erosion resistance. The material with the lowest slurry erosion rate was one containing a Co-Cr binder phase. The addition of chromium increases both the corrosion resistance and the erosion resistance of the cermet.

University of Cape Town

EFFECT OF BINDER CONTENT

The wear rate increased with increasing binder content for a range of WC-Co alloys studied by Shetty, Wright and Stropki [76]. The materials were tested using a slurry velocity of $135ms^{-1}$, an impingement angle of 90° and the test duration was 10 minutes. Work by Pugsley indicated a similar relationship between the binder content and wear resistance [69]. The erosion rate was found to increase with increasing binder content. However it was shown that the grain size of the alloy has a stronger influence on the wear rate than the binder content.

EFFECT OF WC GRAIN SIZE

Work by Pugsley and Allen showed that the slurry erosion of cemented carbides with WC grain size below 1μm is significantly lower than that of the more coarse-grained grades, with erosion taking place preferentially at lower angles in the fine grained materials when compared to the coarse-grained materials [69]. In the case of the fine-grained material the wear process acts on the bulk material with loss occurring as a result of the removal of small flakes of material formed as surface material is smeared in the direction of erodent particle impact. The binder phase and the WC grain respond differently in the coarse-grained materials. There is deformation, crushing and displacement of WC grains and extrusion of the cobalt which is removed preferentially and results in the loss of WC grains which are poorly anchored.

University of Cape Town

3.5.3 THE EFFECT OF ERODENT VARIABLES

SLURRY VELOCITY

The results of Shetty et al. for the 5.1wt%Co and 36.9wt%Co alloys suggest an empirical power-law relation for velocity dependence [76]:

$$\frac{V}{V_s} = Av^b \qquad \text{Equation 3.2}$$

Where A and b are empirical parameters describing the velocity effects of erosion. The alloys showed significant differences in their relative slurry velocity dependence. The low cobalt alloy exhibited a low velocity exponent of 1.66 while the high cobalt alloy had a relatively high exponent of 3.39. This indicates the changes in the erosion mechanism that occur with changing binder content.

SLURRY IMPINGEMENT ANGLE

The relationship between wear rate and impingement angle was qualitatively similar for the high and low cobalt alloys [76].

The erosion rates were a maximum and approximately constant between an impingement angle of 50° to 90°. Below 50° the wear rates decreased rapidly. Therefore even though the mechanisms in the high and low cobalt alloys differed the wear rates exhibited a similar angular dependence

University of Cape Town

CHAPTER 4

LITERATURE REVIEW

WC-Co COATINGS

4.1 INTRODUCTION

The thermal spray process is very versatile allowing components of all shapes and sizes to be coated. As a result WC-Co coatings are used in a wide range of applications for the protection of surfaces from all types of wear, examples include, compressor piston rods, pump plungers, shaft sleeves on centrifugal pumps and fans, and midspans of compressor blades in gas turbines. A variety of spray systems are available resulting in coatings that vary in their wear performance.

The objectives of the following chapter are to describe the different types of spray processes available and previous work done on the wear performance of WC-Co coatings, with particular emphasis on the factors that affect the wear resistance of these coatings.

University of Cape Town

4.2 THE THERMAL SPRAY PROCESS

In general the coating is formed by particles of liquid material (molten powder particles) that strike against the substrate where they form thin platelets called lamellae, also known as splats, which cover surface irregularities. The lamellae undergo rapid cooling and rates of $10^6 Ks^{-1}$ have been observed. The cooling rate depends on the particular spray system used [78]. The solidification front moves progressively through the lamellae away from the substrate which acts as a heat sink. The high kinetic energy on impact is converted into additional heat which enhances the production of localised metallurgical and mechanical bonds with the substrate and also between the coating particles [79, 80].

4.2.1 THE DECARBURISATION OF WC-CO

Thermal decomposition or decarburisation of WC occurs during the thermal spraying of WC-Co powders. The decarburisation is followed by the formation of complex carbides of the type: $Co_xW_yC_z$ such as Co_3W_3C and $Co_9W_9C_4$, these compounds are brittle in nature and therefore undesirable and detrimental to the coating performance. The decomposition of WC is a two step mechanism, the first reaction involves the decomposition of WC to W_2C followed by the oxidation assisted decarburisation of W_2C to metallic tungsten [81]:

$$2WC \rightarrow W_2C + C \qquad \text{Eqn. 4.1}$$

$$W_2C \rightarrow 2W + C \qquad \text{Eqn 4.2}$$

Loss of carbon in WC-Co coatings may also occur by the diffusion of carbon into the matrix or by oxidation in the flame according to the following reaction:

$$2C + O_2 \rightarrow 2CO_g \qquad \text{Eqn. 4.3}$$

The overall reaction is kinetically driven i.e. time and temperature dependent, making the degree of decarburisation sensitive to the deposition process flame temperature and flame velocity [82, 83]. Decarburisation may therefore be reduced by adjusting the flame condition but cannot be totally eliminated.

The main thermal spray processes in use are Atmospheric Plasma Spraying (APS), Detonation-gun (D-Gun), and the High-Velocity Oxy-fuel (HVOF) processes. The D-Gun and HVOF processes produce a high velocity and moderate temperature combustion flame (velocity >1000ms^{-1}, temperature< 3000K). Both these processes have higher particle impact velocities and lower temperatures than the APS process and are therefore ideal for depositing WC-based materials [84].

The extent of WC transformation during spraying depends on the powder type, the type of spray process and the amount of oxygen in the environment and the

University of Cape Town

spray parameters [81]. In the plasma process there is more thermal energy available to drive the decomposition process. In the HVOF process it has also been shown that an increase in the flame temperature leads to higher levels of decarburisation. Generally, decreasing the flame temperature and increasing the gas velocity limits the extent of decarburisation.

4.2.2 THE PLASMA SPRAY PROCESS

Plasma is the term that is used to describe a gas that has been raised to such a high temperature that it ionises and becomes electrically conductive. When plasma spraying, the plasma is created by an electric arc burning within the nozzle of a plasma of a gun. The arc gas is formed into a plasma jet as it emerges from the gun nozzle. Powder particles are injected into this jet where they melt and then strike the surface at high velocity to produce a strongly adherent coating. Almost any material can be sprayed including metals, ceramics and plastics. The workpiece (substrate) remains cool because the plasma is localised at the gun. Air plasma spraying uses an inert gas plasma and the temperatures is >15000K [45]. It is ideal for depositing ceramics and alloys. It is also widely used for carbide coating but the high temperatures can lead to decomposition of WC.

University of Cape Town

4.2.3 THE DETONATION GUN PROCESS

The Coating material in powder form is metered into the barrel and combined with a precise mixture of gases. The gas mixture is detonated with an electrical spark, heating and accelerating the powder down the barrel, propelling it at supersonic velocities onto the part being coated. Typical gas temperatures are between 2500K and 3100K and the particle velocities are approximately 800ms^{-1}. This is a form of high pressure, high velocity flame spraying producing dense and uniform coatings with extremely high bond strength [85].

4.2.4 THE HIGH-VELOCITY OXYFUEL PROCESS (HVOF)

High velocity oxy-fuel gas flame spraying was commercially developed as the Jet-Kote process in 1986 [86, 64] and has been developed into several different types of commercially available spray guns.

Liquid fuel and oxygen are fed via a pre-mixing system at high pressure into a combustion chamber where they burn to produce a hot, high pressure gas stream. This is expanded through the nozzle to increase the gas velocity to around 1500ms^{-1} and the pressure to slightly above atmospheric pressure. At this stage the powder is injected into the gas stream. The gas stream heats and accelerates the powder particles causing them to impact with tremendous energy on the substrate surface.

University of Cape Town

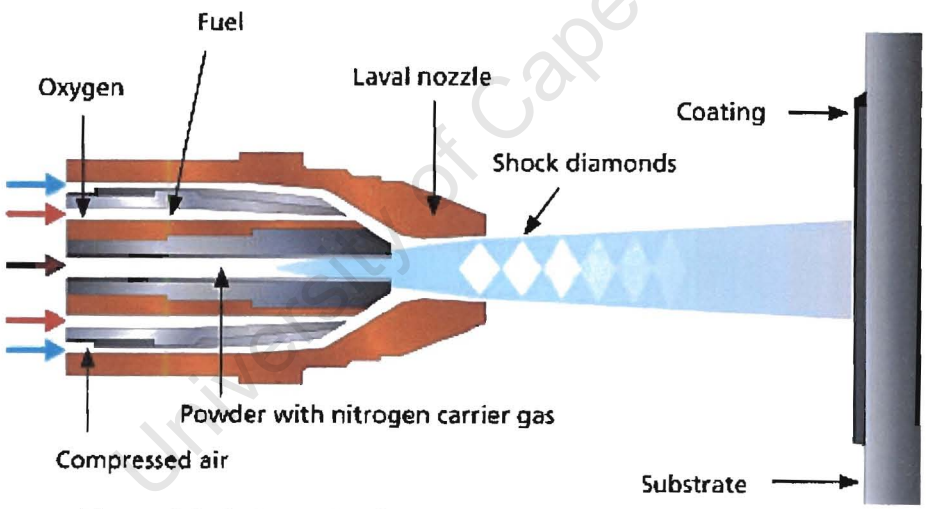

Figure 4.1: Schematic of the High velocity oxyfuel process

4.3 COATING STRUCTURE

Due to the nature of the thermal spray process the final coating structure is very inhomogeneous with a high frequency of imperfections as illustrated in Figure 4.2.

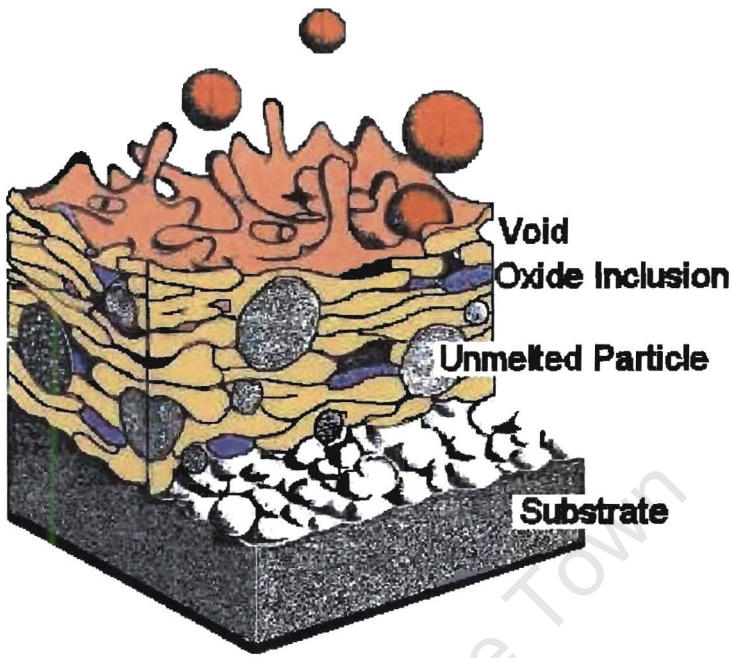

Figure 4.2: Schematic of a Thermal Spray Coating

Porosity, as a result of entrapped gases, is frequent and phase variations result from incomplete melting of the powder. The porosity is increased with an increase in the grit size of the precursor powder. The cobalt binder phase normally exhibits a lamellar structure. However, in the case of HVOF sprayed coatings, the microstructure is closer to that of a sintered hard metal [45].

Thermally sprayed coatings normally contain a non-uniform carbide density distribution which leads to a mean free path that is somewhat larger than that in sintered product which has λ values between 0.1 and 1.0μm with typical grain sizes of 1.0μm [87].

The inherent anisotropy of thermally sprayed coatings results in anisotropic mechanical properties such as fracture toughness which is considerably lower parallel to the coating / substrate interface than perpendicular to it [88, 89]; this influences the erosion behaviour of the coating.

University of Cape Town

4.4 EROSION OF WC-CO COATINGS

The anisotropic structure of WC-Co coatings results in an inferior wear performance when compared to their sintered counterparts [86]. The high levels of defects and porosity in the coatings have a detrimental effect on the coating performance under wear conditions. Wayne and Sampath have compared the wear performance of sintered and thermally sprayed WC-Co materials and concluded that the erosion resistance of the sintered material is twice as great as for the thermally sprayed product under air/sand jet impingement conditions, with a velocity of 110ms^{-1} and at an impact angle of 90° [88]. The porous structure of coatings leads to weak intersplat and carbide/matrix bonds, which lowers the fracture toughness and hardness of the coating decreasing its erosion resistance [88, 89].

Cermet coatings have been found to be very sensitive to the carbide grain size and volume fraction of the binder phase as expected in these types of materials [90]. These two factors determine the distribution of the wear resistant WC phase in the coating and hence determine the effectiveness of the material in resisting wear. The angle of impact, the size of the erodent particle and the velocity of impact all influence the ideal binder content and binder phase for optimum erosion resistance. The sensitivity of the coating to these various parameters has led to investigators obtaining results which at first glance appear contradictory to previously published data.

University of Cape Town

4.4.1 EROSIVE WEAR MECHANISMS

Work by Verdon et al showed a linear dependence of weight loss as a function of time, for periods of several hours during solid particle erosion [91]. Three erosion mechanisms were evident from scanning electron microscopy studies. Firstly, a ploughing mechanism that removes the binder phase and is followed by loss of WC similar to that observed by Wood et al on the WC-Co-Cr investigated in their study [89]. The second mechanism was a process of delamination, in which crack propagation takes place across the binder and along island boundaries.

The third active wear mechanism was the corrosion of the binder, which accounted for a small amount of the wear taking place. The dominant mechanism was found to be the first one at a low flow velocity of less than $90ms^{-1}$ and when the flow velocity was higher than $140ms^{-1}$, the wear was a combination of ploughing of the binder in one of the coatings and delamination in the second coating studied.

An interesting feature of the work by Verdon et al. was that local heating of the specimen under tangential erosion occurred and led to melting of the erodent particles. In these experiments the erodent used was collected from the runners of a hydraulic dam.

4.4.2 Effect of Binder Phase

Hawthorne et al. carried out erosion tests on 10 HVOF sprayed coatings [92]. The test conditions used were dry jet and slurry jet erosion using alumina as the erodent particles, at two different impact angles. The dry tests involved particle velocities of $84ms^{-1}$ and in the slurry tests the particle velocities were only $15ms^{-1}$. The results indicated a much higher wear rate for the dry test conditions, the effect of the higher erodent impact velocities. For the dry tests the particle velocities is equivalent to the air stream velocity, but in the case of the slurry tests the particle velocities are lower than the impingement velocity of the water as a result of the fluid dynamics. The best slurry wear resistance was exhibited by the coating with a Cr-Ni binder.

There was strong evidence of selective removal of the binder in the coating containing pure cobalt. The corrosion potentials of the coatings were evaluated and the coating with pure cobalt binder was found to be the more susceptible to corrosion than that with a Co-Cr binder phase.

The WC-12wt%Co coating exhibited the best performance in both dry erosion and slurry erosion conditions when the erodent particles were large. However, with small particles this changed and WC-20wt%Co-4%Cr had the best

University of Cape Town

performance at an impact angle of 90° while the WC-20wt%Cr-6wt%Ni had the best performance at 20°.

Toma et al. studied six different thermal spray coatings, four of the coatings were carbide coatings and the other two were chromium oxides [93]. The coatings were tested using silica with a grain size of between 100 and 500μm for a 48 hour duration. The WC-Co material had the poorest wear resistance. The addition of 4wt%Cr improved both the erosion and corrosion resistance of the WC coating.

Bjordal et al. investigated the wear of four different thermal sprayed coatings, consisting of carbide particles in different matrices with a duplex stainless steel (SAF 2205) as the reference material [94]. The WC-Co material suffered a much higher material loss than the coating containing a mixed Co-Cr binder. The combined erosion and corrosion of the WC-Co coating gave rise to a synergistic effect under the slurry conditions in which the materials were tested. The addition of Cr to the Co binder caused a significant improvement in the corrosion of the material, however at high erosivities it is expected that erosion will dominate, making the corrosion properties less important.

Another study carried out by Berget et al. compared the erosion and corrosion properties of WC coatings and duplex steels in sand-containing synthetic sea water [95]. The results showed the poor wear resistance of the coating containing the pure Co binder which was highly inferior to the stainless steel, which was not recommended for use under corrosive conditions.

The relative wear resistance was calculated as the ratio of the volume loss of the 13-4 steel to that of the coatings at steady state erosion by Karimi et al. [90]. The benefits of the coatings in terms of improved wear resistance are more pronounced at higher flow velocities As in the work of Hawthorne, the coating containing a Co-Cr binder performed better than the pure cobalt binder, again emphasising the importance of a corrosion resistant binder under erosive-

University of Cape Town

corrosive conditions. In addition to improving the corrosion resistance of the binder, chromium aids the formation of favourable microstructures which provide toughness and enhance the binding of the carbide particles. Furthermore, the presence of Cr increases the volume fraction of binder leading to an optimal ratio of WC to binder phase, resulting in a more efficient WC distribution in the coating.

4.4.3 Effect Of WC Grain Size

The work of Berget et al. also looked at the effect of the binder phase and WC grain size on the erosion and erosion-corrosion of WC based coatings [95]. Accordiing to Berget et al. small WC particles are beneficial for both pure erosion and erosion corrosion. In the coatings investigated in their study a decrease of the average WC grain size from 5µm to 2.5µm more than halved the material loss and a further decrease from 2.5µm to 1µm also further enhanced the erosion and erosion-corrosion resistance. The finer WC structure is thought to limit the removal of any WC caused by impact.

4.4.4 Effect Of Coating Structure

Wood et al carried out studies on the sand erosion performance of detonation gun applied WC-Co-Cr coatings [85], and found that the presence of cracks and voids in the coating accelerate the erosion process as they aid crack initiation and growth. The results for the LW45 WC-Co-Cr. material for the low energy tests showed a transition of the wear rates from a constant low wear rate to a much higher constant wear rate and this is due to the two operating wear mechanisms taking place. Up to a testing time of 180 minutes the wear rate was $1.61 \times 10^{-3} mm^3 min^{-1}$ above that erosion time the wear rate increases to $12 \times 10^{-3} mm^3 min^{-1}$ which is about 10 times the initial wear rate. A similar transition was observed for the high energy test, however in this case the initial rate of $0.43 mm^3 min^{-1}$ was higher than the second rate after the transition point. The initial wear rate under high energy conditions is approximately 36 times greater than that at low energy conditions. This is because the stresses induced in the coating upon particle impact differ. Under high energy conditions, there is

University of Cape Town

rapid crack growth, leading to spalling which happens almost immediately once the test is started. In the low energy test the crack growth is slower and requires a greater number of particle impacts before cracks interlink and cause spalling of the material.

Two wear mechanisms were observed on the LW45 WC-Co-Cr material tested. These were cutting and gouging, which are dominant mechanisms in ductile material such as the binder and a cracking mechanism was also observed, typical of brittle materials. The mechanism was found to be dependent on the angle of attack and the associated energy of the particles. In the first mechanism, microcutting and ploughing of the soft binder results in exposure of the WC particles, which are then poorly supported and can then be gouged out by the impact of the eroding particles as they strike the material surface. In the second mechanism particle impact causes fluctuating stress that leads to the propagation of sub surface cracks by a fatigue mechanism resulting in a micro-cracked coating. Crack initiation occurs at coating defects and when cracks interlink larger areas of the coating are removed in sizes ranging from 10-400μm. The first mechanism occurs at low impact angles and low particle energy i.e. the particles have insufficient momentum to cause sub surface crack growth.

Wood et al concluded that the erosion rate of the sprayed material was found to be comparable to that of the sintered material for low energy impacts but at high-energy impacts the sintered material out performed the sprayed material by a factor of 4.

4.4.5 Effect of Coating Hardness

The HVOF coatings studied by Hawthorne et al. indicated a direct relation between the coating hardness and the erosion resistance at both a low impact angle of 20° and a high impact angle of 90°, however, in some cases the wear rate has been found to increase with increasing coating hardness [92, 81]. Nerz et al. associated an increased hardness with a lower retained carbide content

University of Cape Town

and the formation of brittle phases during spraying. Therefore the carbide content was considered to be more important than the coating hardness.

4.5 Summary Of The Factors That Affect The Coating Performance

A large number of variables affect the quality of the thermal spray coatings, including the spray process used, the powder type and other variables described below.

4.5.1 The Manufacturing Route Of The Powder

There are a variety of powder manufacturing routes that are available and the powders produced differ in morphology, crystal structure and tungsten carbide grain size, powder grain size and also the carbon and cobalt content [87]. The various manufacturing routes for powder production include: Cast-crushed; sintered-crushed; agglomerated; aggregated; coated.

In the work of De Villiers et al. a sintered and crushed powder gave the best erosion results for both the 17%Co and the 12% Co coatings studied [96]. However the powder type was found to have a small effect when compared to the effect of the coating composition.

4.5.2 The Powder Grain Size Distribution

The coating quality is also sensitive to the particle size range. A narrow particle size range is important for the application of a uniform coating and also to improving coating machinability, grindability and in-service performance. Too broad a size distribution will negatively affect the deposit efficiency and coating quality. Berget et al. found that a narrow size distribution produced coatings of higher quality than powders with wider grain size distributions [97]. The reason being that powder grains of different sizes have different heating and acceleration behaviour. Small grains overheat more easily than larger grains, which may lead to phase changes that are detrimental to the wear resistance of the coating.

University of Cape Town

4.5.3 THE POWDER PARTICLE SIZE

Particles need to be sized to match the specific thermal spray process for which they will be used. Particles that are either too big or too small hinder the flow of the feedstock and have a negative effect on the strength and homogeneity of the coating and also lead to increased porosity. When the nominal particle size is matched correctly to the spray gun, the melting of the powder is optimised, this improves the coating quality and increases the deposit efficiency leading to a reduction in material waste.

4.5.4 THE PARTICLE SHAPE

The particle shape has an effect on the final structure of the coating produced. Angular powders have a tendency to feed poorly and erode the internal components of the spray gun at an accelerated rate. Spherical powders, produced by the agglomeration process, reduce spare part costs and coating downtime. Consistent powder feed is important for uninterrupted spraying operations and repeatable coatings.

University of Cape Town

4.5.5 THE SPRAY PROCESS

The wear performance of WC-Co coatings sprayed by the HVOF process is better than that of the plasma and detonation gun processes [98]. The HVOF process produces coatings of the best quality with minimum porosity, high adhesion and low oxide content due to the high particle velocity and lower flame temperature.

4.5.6 THE STRUCTURE OF THE COATING

Coatings with a more homogeneous and denser structure generally perform better than badly structured coatings in abrasion and erosion. Fine grained coatings containing few or no pores and micro cracks are preferred in erosion applications [99].

4.5.7 THE WC GRAIN SIZE

A coating must retain a large volume fraction of finely distributed WC to achieve the best possible performance against wear. The erosion and erosion-corrosion resistance of WC-Co-Cr coatings increases with decreasing WC size from 5-1μm for the same binder content [95]. The reason for this is that the mean free path of the matrix is reduced, resulting in greater constraint and increased hardness. Therefore there is less exposure of the ductile matrix to the abrasive particles as a result of a more homogeneous composite structure. Large WC particles have a tendency to rebound off the substrate during spraying resulting in a lower deposition efficiency compared to that obtained with powders containing finer WC particles.

4.5.8 THE BINDER PHASE

If the coating is to be used in both a corrosive and erosive environment the corrosion properties of the binder metal must be taken into account. A binder metal of pure Co will suffer from corrosion if exposed to a corrosive environment. Combined erosion and corrosion gives rise to a synergistic effect [97]. When a highly corroding matrix is present such as in the case with pure cobalt binder, the matrix corrodes and undermines the carbide particles, which then fall out more easily [93]. In addition, the corrosion properties of the material in contact with the coating must also be taken into account. Large differences in the corrosion properties of the material in contact with the coating may lead to galvanic effects which could have a detrimental effect on the coating/substrate system. Chromium is added in order to enhance the corrosion resistance of WC-Co coatings. The Co/Cr binder phase improves the corrosion resistance several times compared to a Co binder phase and also increases the erosion resistance of the coating. In some cases nickel may also be added to improve the corrosion resistance.

University of Cape Town

CHAPTER 5

EXPERIMENTAL PROCEDURE

5.1 MATERIALS

The coating materials and feedstock powders that were studied in this work were supplied by Thermaspray, a company that forms part of Technovet (Pty) Ltd.

5.1.1 FEEDSTOCK POWDERS

Two powders were supplied by Praxair-Tafa in the agglomerated and sintered condition with a grain size which varied between 15 and 45μm. A third powder was supplied by Sulzer Metco which was sintered and crushed to a size range between 11 and 45μm. The nominal compositions of the powders are shown in Table 5.1.

University of Cape Town

Table 5.1: Nominal compositions of powders and coatings

Material	WC (wt%)	Co (wt%)	Cr (wt%)	Nominal Density (kgm^{-3})	Spray Method
WC-12Co	88	12	0	1497	JP-5000
WC-10Co-4Cr	86	10	4	1477	JP-5000
WC-10Co-4Cr	86	10	4	1477	DJ Std
WC-10Co-4Cr	86	10	4	1477	DJ New

5.1.2 COATING MATERIALS

The four coatings evaluated were produced using two different HVOF spray systems. The nominal compositions of the coatings are shown in Table 5.1. Two of the coatings were produced using a TAFA JP5000 HVOF system. The combustion gases were kerosene and oxygen, with a nominal powder consumable size of 20-50 μm. The other two coatings were sprayed using a

Sulzer Metco DJ2700 HVOF system with propane and oxygen as the combustion gases. The coatings were all sprayed onto a mild steel substrate to a thickness of approximately 200 μm.

5.1.3 SINTERED MATERIAL

Sintered tungsten carbide was used as a reference material. The nominal composition of the material was 90wt% WC and 10wt% Co. The material was previously characterized as follows: WC grain size was 2.9 μm, the mean free path was 0.90 μm and the density was 14.5 gcm^{-3} [50].

5.2 DRY EROSION TESTING

Room temperature dry jet testing was performed, in an apparatus which allowed the impingement angle and particle velocity to be varied. A schematic of the apparatus is shown in Figure 5.1.

The main components of the erosion rig are the chamber in which the sample is placed, a feeder funnel and a venturi tube. The feeder funnel is placed with its opening above the groove in the turntable and the erodent falls into the groove and is drawn up by the venturi tube. A voltmeter attached to the motor allows the speed of the turntable to be varied and adjustment of the compressed air stream using a regulator allows the particle velocity to be varied. A gauge attached to the regulator gives the air pressure reading.

University of Cape Town

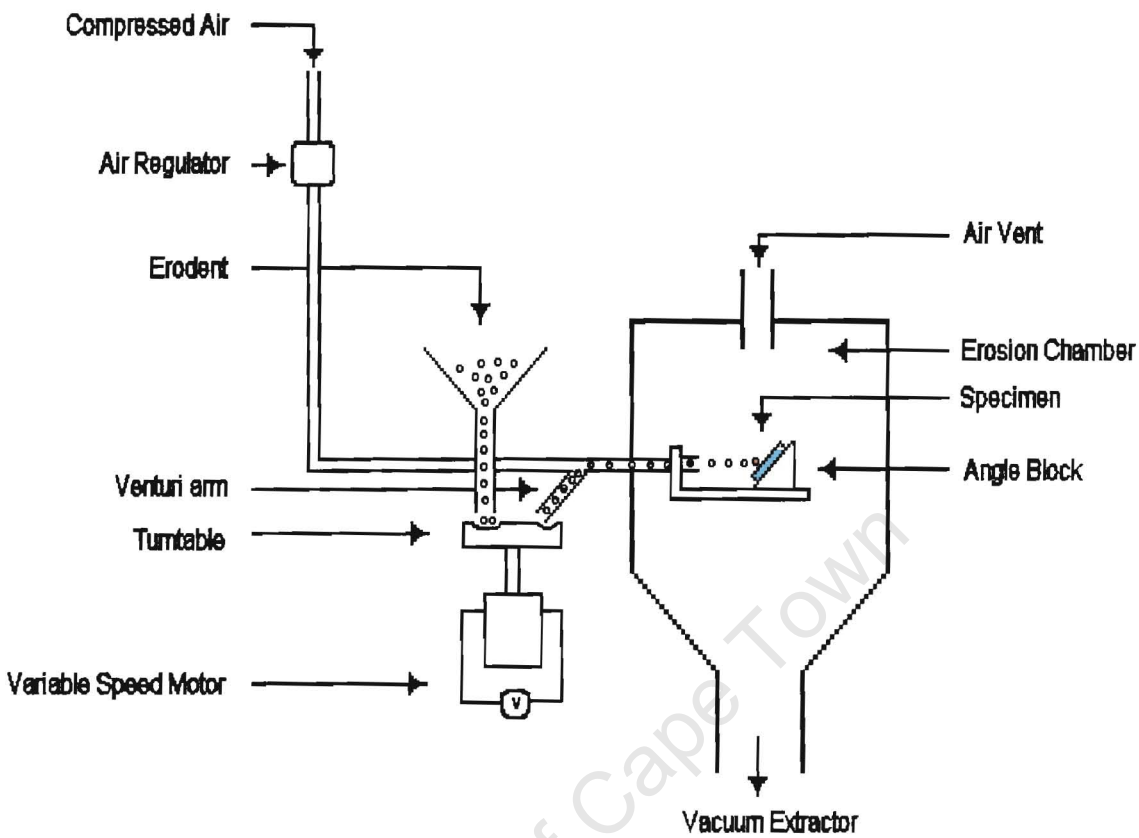

Figure 5.1: Schematic of the dry erosion apparatus

University of Cape Town

The sample is placed on an angle block (whose angle can be varied, as shown in Figure 5.2) and attached to the specimen stage, which is positioned in the chamber during testing. A vacuum extractor unit removes the used erodent through the bottom of the chamber.

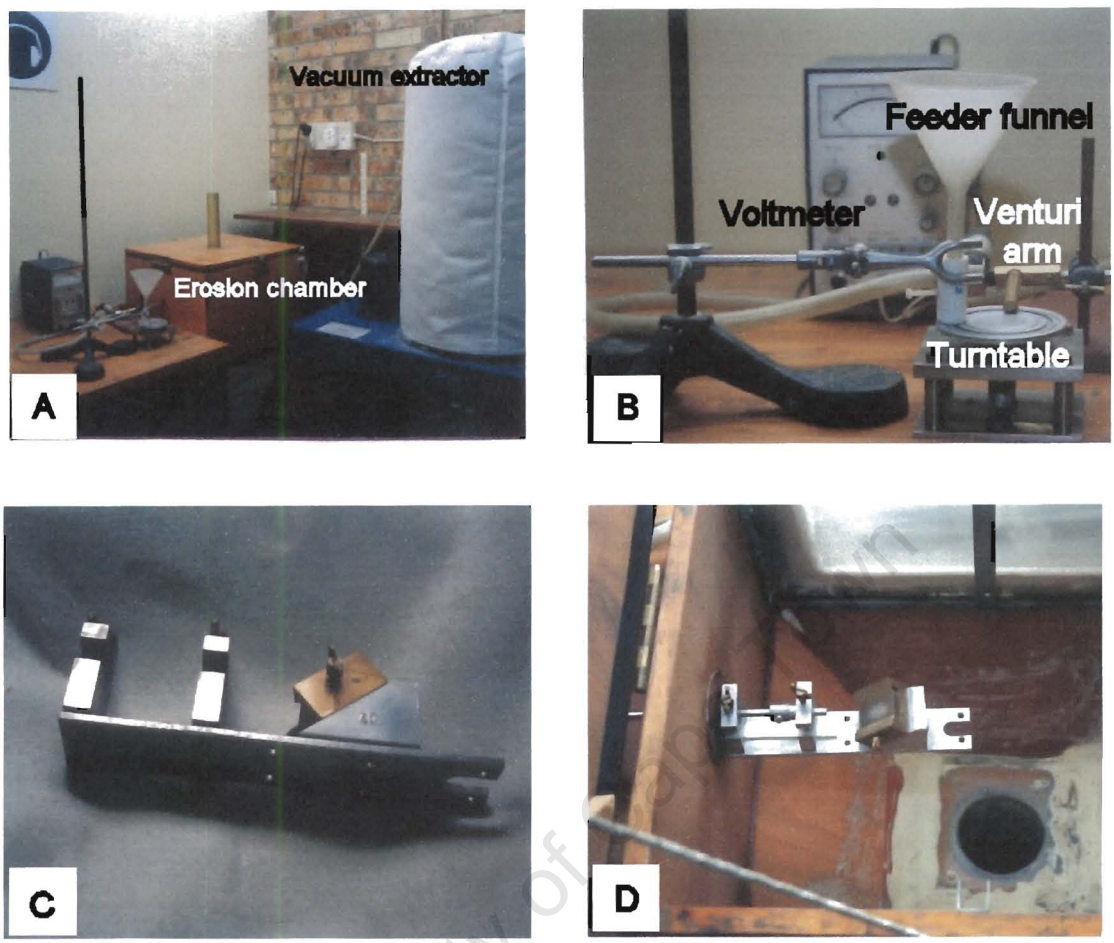

Figure 5.2: (a) Setup of the apparatus, (b) Erodent feed system, (c) Specimen mounted on a 40° angle block and (d) sample positioned inside the erosion chamber showing wear on the surface

University of

Specimens, approximately 25mm square and 6mm thick were machined from the coated mild steel strip. The sintered material was received in the form of blocks 22mm long, 20mm wide and 4mm thick.

Before testing all the samples were unltrasonically cleaned in alcohol, dried and kept in a dessicator prior to any weighing on a balance which was accurate to 0.01mg.

Specimens were placed in the apparatus and eroded with silica particles.

For these tests the erodent used was silica (SiO_2) supplied by Consol Industrial Minerals. The particle size distribution of the silica as supplied by the manufacturer is shown in Table 5.2 and the morphology is shown in the micrograph in Figure 5.3.

Figure 5.3: Silica used as the erodent in the erosion tests

Table 5.2: Size distribution of silica erodent

PARTICLE SIZE (µm)	PERCENTAGE
Greater than 150	3.8
150	38.7
106	38.6
75	17.7
Below 75	1.2

University of Cape Town

The mass loss suffered by the coating after each 40g sample of SiO_2 passing through the apparatus was measured to an accuracy of 0.01mg following cleaning in alcohol. Each sample was eroded with a total of 320g of silica and the weight loss converted to volume loss. The wear rate was calculated from the straight line portion of the curve as mm^3g^{-1}.

5.2.1 EFFECT OF IMPACT ANGLE

The initial tests carried out were conducted to determine the effect of impact angle on the wear resistance of the coatings. The specimens were mounted on the angle block and attached to the specimen stage at fixed angles of 30°, 45°,

60°, 75° and 90°. The particles were propelled at 66 ms^{-1} from a 5.96 mm diameter, 23 cm long barrel onto the target coatings positioned 50 mm from the nozzle.

5.2.2 Effect Of Erodent Particle Velocity

These experiments were conducted to determine the erosion rate of the DJ (New) WC-Co-Cr coating at a 60° impingement angle over a range of erodent particle velocities. The coating was tested at the following erodent velocities: 20ms^{-1}, 29ms^{-1}, 36ms^{-1} and 66ms^{-1}, the velocities were controlled by regulating the air pressure in the venturi tube. The erodent used was SiO_2 with the particle size distribution shown in Table 5.2.

5.2.3 Effect Of Erodent Particle Size

In these experiments the DJ (Standard) WC-Co-Cr coating was tested at an impact angle of 60° with a particle velocity of 66ms^{-1}. The series of tests were conducted using SiC as the erodent (Figure 34). SiC was available in a wide size range compared to the SiO_2 therefore SiC was used as the erodent. The erodent particle sizes that were used were 106-125μm, 425-500μm, 600-710μm. This test also allowed the effect of erodent particle hardness to be assessed by comparing the results with those obtained with the softer SiO_2 erodent, for tests involving particles of similar size.

University of Cape Town

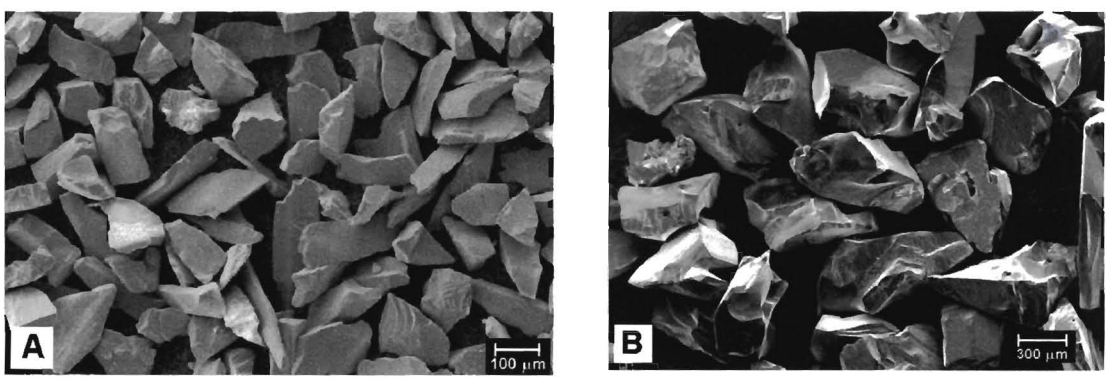

Figure 5.4: SiC used at the erodent in the dry erosion tests; a: 106-125μm b: 425-500μm

PARTICLE VELOCITY CALIBRATION

The velocity of the erodent particles was determined using the rotational disc method [100].

The apparatus consists of two thin discs connected by a common shaft as shown in Figure 5.5. The two discs rotate a fixed distance apart with the same angular velocity. The front disc has a slit cut into it. A variable speed motor allows the speed and direction of rotation to be controlled and an electronic counter gives the angular velocity in revolutions per second. The rotating discs are positioned in front of the erodent particle stream, which passes through the slit in the front disc and erodes the second disc. When the rotation direction is changed another erosion mark is made on the second disc. The separation between the erosion marks is measured using a vernier calliper and related to the particle velocity.

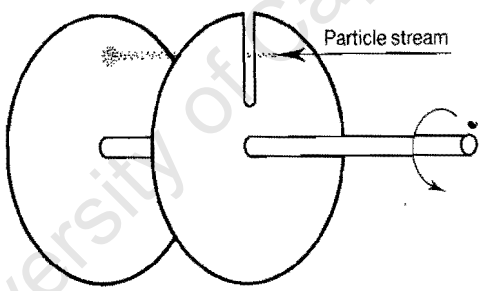

Figure 5.5: Schematic illustration of the double-disc method of measuring the particle velocity in gas-borne particle erosion experiments

University of Cape Town

The velocity of the particles was calculated using the following equation:

$$V = 4 \pi r U L / \sigma$$

Where: V is the average particle velocity

r is the radius from the disc centre

U is the rotational velocity of the disc

L is the distance separating the two discs

σ is the linear separation of the two markings

The two discs used in this work had a radius of 2.17 cm and the separation between them was 1.89 cm. The split discs were placed 10 cm from the nozzle end and rotated at a speed of 40 revolutions per second (rps). An erodent particle stream was passed through the nozzle for 2 minutes as the discs were rotated in the clockwise direction. The particle stream was stopped and the speed reduced to zero before the rotational direction was reversed. Once the direction had been reversed, the rotational speed was increased to 40 rps and the particle stream was passed through for a further two minutes. The separation of the erosion marks produced was measured using a vernier calliper. This was repeated for several air pressures between 0.5 and 3.0 bar. The air pressure was plotted against velocity and a best fit line was obtained for the pressure/velocity relationship.

University of Cape Town

5.3 Slurry Erosion Testing

Slurry erosion testing was carried out using a jet impingement rig that was previously used by Pugsley and earlier built and used by Wentzel [7, 76]. The rig design is based on the original rig of Zu and is shown schematically in Figure 5.6 [101]. The coatings were tested at nominal impingement angles of 45°, 60°, 75° and 90°.

During operation, the carrier fluid is pumped from the holding tank to the ejector. The difference in diameter between the input and output nozzles creates a low-pressure region which allows erodent to be sucked up a vertical tube into the ejector. The erodent and carrier fluid are mixed forming a slurry which is accelerated through the ejector and impinges on the surface of the specimen. The slurry then falls back into the funnel and is separated into the erodent and carrier fluid by means of a gravity filtering system; the erodent particles sediment out and the carrier fluid overflows into a second container. The carrier fluid then overflows into the holding tank and any entrained erodent particles remain in the second container. The entire cycle then repeats itself and the extent of erosion is monitored by periodic mass loss measurements.

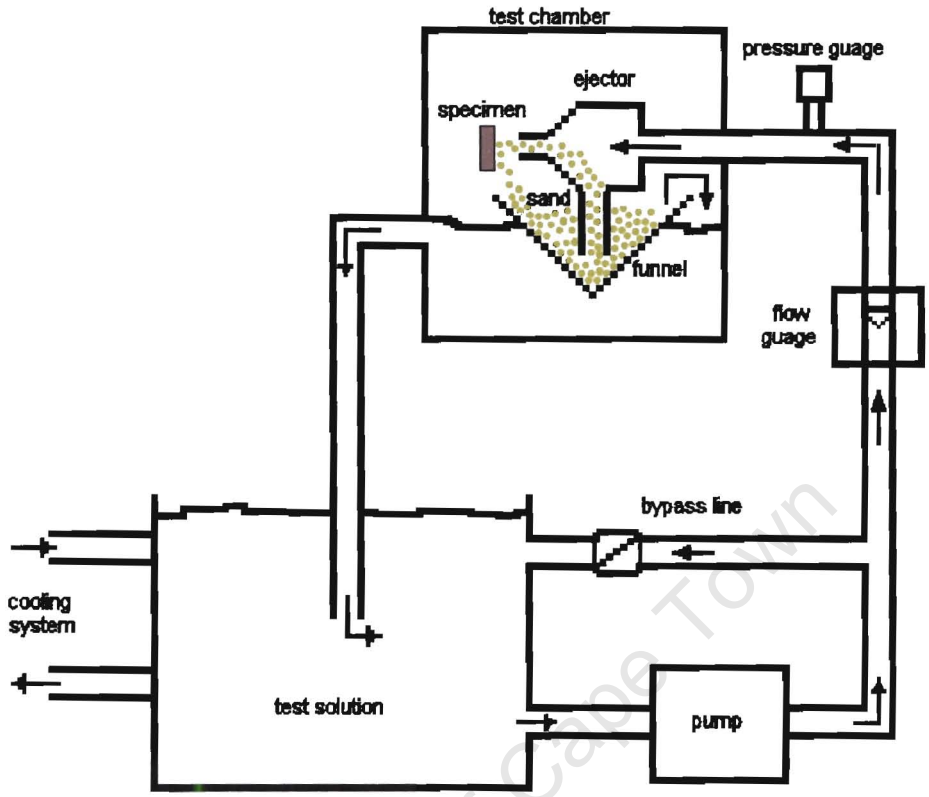

Figure 5.6: Schematic of the slurry rig.

In order to prevent heating of the carrier fluid during extensive operation, a cooling coil was inserted in the rig through which tap water was circulated. Erodent degradation of the erodent was monitored by Wentzel who found that no significant degradation occurred after four hours of testing. Therefore in this work the erodent was replaced after every four hours of testing.

University of Cape Town

Figure 5.7: The slurry jet erosion rig

University of Cape Town

CALIBRATION

The impact velocity and the sand concentration were determined by collecting the slurry leaving the exit nozzle for a known period of time, which was measured with a stop watch. The impact velocity was derived from the measured cross-sectional area of the exit nozzle and the volume of slurry collected. It is assumed that the velocity of the erodent particle is equivalent to that of the water. The particle weight concentration in the slurry was calculated by weighing a known volume of slurry.

The holding tank of the slurry rig was filled with 200 litres of tap water and two kilograms of unused silica sand were washed in tap water and placed in the funnel. The erodent particle size was as indicated in Table 5.2 and the concentration in the slurry was 11wt%.

The samples used for slurry erosion testing were in the form of round mild steel coated discs. The diameter of the disc was 18mm and the thickness was 20 mm. The samples were cleaned ultrasonically in alcohol and dried and weighed to an accuracy of 0.01mg before testing.

The specimen was then placed in the specimen holder at the required impact angle, and secured to the chamber. This positioned the specimen at a distance of 30mm from the output nozzle which had a diameter of 5.3mm. Slurry was directed at the specimens at $7ms^{-1}$ with a flow rate of 9 $lmin^{-1}$ for 10 minutes, after which they were removed, cleaned ultrasonically in alcohol, cooled and weighed. This was repeated until the test time of 1 hour had been reached.

The test time that was used was determined by carrying out preliminary tests on the materials in order to determine the ideal testing time that resulted in a significant wear loss.

The wear rate was reported as volume loss per minute.

5.4 Corrosion Testing

The corrosion tests were carried out according to the ASTM standard test method, designated as G5.

A test solution of one litre of 1.0N H_2SO_4 was prepared by diluting 27.8ml of 98% H_2SO_4 in distilled water and mixing with a magnetic stirrer. The solution was then poured into a 900ml test cell. The test cell was placed into a temperature-controlled water bath of 30 ± 1°C. A high density graphite auxiliary platinum electrode was then inserted into the bath, followed by the insertion of a standard calomel electrode (SCE). The solution was then purged using argon gas for 30-40 minutes before the specimen holder was inserted. The system was purged with argon throughout the duration of the test.

University of Cape Town

The specimens were cleaned prior to immersion in the cell by degreasing for five minutes in boiling benzene and rinsing in distilled water. The specimens were then mounted in the holder and used within one hour of preparation.

The working electrode (specimen holder) was transferred into the solution and the SCE was placed 2mm from the specimen surface. The experiment was only initiated after an immersion period of 55 minutes. Potentiodynamic scanning was carried out at a rate of $0.167mVs^{-1}$ from 250mV below the free corrosion potential up to 1.65V.

5.5 Microstructural Characterization

5.5.1 Scanning Electron Microscopy

During powder processing and thermal spraying, microstructural modifications take place in the material as previously discussed in section 4.3. In order to observe any structural changes that might have taken place, the microstructure of the initial powders and the sprayed coatings were examined. The wear scars formed on the target materials after dry and slurry testing were also examined.

University of Cape Town

Powder Morphology

The surface morphology of the powders was examined using a Leica Stereoscan 440 Scanning electron microscope with the following settings: 10kV accelerating voltage; 50pA current probe; 24mm work distance; 0° tilt. The samples were prepared by sprinkling a little powder onto double sided carbon tape placed on an aluminium metal stub. The samples were studied at low and high resolutions, which allowed for the overall morphology to be examined and also allowed for a close-up study of individual particles.

For cross-section morphology, a few milligrams of each powder were mounted in 15ml of Specifast resin using a Struers labPress-1. The resin was cured under 15kN at a temperature of 180°C for 6 minutes and subsequently cooled for 8 minutes using a low water flow rate. Each mounted sample was then polished to

a 1 micron finish. Energy Dispersive X-ray analysis (EDX) was used for qualitative analysis, in order to distinguish the different phases and to give a map of the dispersion of the various elements. The WC grain size was determined by linear measurements of the grains.

COATING MICROSTRUCTURE

A specimen of coated mild steel was mounted in a conductive iron resin and then cured at a pressure of 5kN for 5 minutes. Each mounted sample was then polished to a 1 micron finish. The mounted samples were examined using a Leica Stereoscan 440 SEM with the following settings: 10kV accelerating voltage; 50pA current probe; 24mm work distance; 0° tilt. EDX was utilized for elemental analysis.

Some of the eroded samples were mounted onto metal stubs and the worn surface examined from the top of the surface, while in the other samples, transverse sections through the wear scar were taken, mounted and polished to a 1 micron finish for SEM examination.

University of Cape Town

5.5.2 X-RAY DIFFRACTION

X-ray diffraction of the powder feedstock and the coatings was performed on a Phillips diffractometer. Copper K_α-radiation was used and the samples were run from 20°-100° (2θ), with a step size of 0.02° (2θ) and a fixed time of 2 seconds per step.

5.5.3 MICROHARDNESS

The Vickers microhardness of the coatings was determined using a Matsuzawa MXT-α7 digital microhardness tester. The samples were loaded in cross section with a standard Vickers diamond indentor using a force of 1kg. The measurements were taken in the middle section of the coating to avoid any edge effects. The indentations were spaced far apart to prevent the deformation from one indentation affecting any other results and some readings were rejected

where the indent was distorted. At least ten measurements were taken for each coating.

5.5.4 PARTICLE SIZE DISTRIBUTION

The Malvern Mastersizer^{TM} laser light scattering method was used to determine the size variation in the powders. In this method a powder sample of 5-15g is dispersed in water and circulated through a 15ml measuring cell where it is intercepted by a beam of laser light. The light is scattered by the powder particles producing diffraction rings. The scattering angle is dependent on the particle size and from the intensity of the various rings produced it is possible to determine the particle size distribution. The Malvern 2600 Powder Module was used for the analysis.

University of Cape Town

CHAPTER 6

RESULTS

6.1 INTRODUCTION

Coatings are produced as outlined in section 4.6 by thermospraying powders. These powders are produced by consolidating together WC and a binder material into a size that is suitable for spraying. The influence of the WC grain size and the homogeneity of the powders has an important influence on the subsequent structure and properties of the coating. It is therefore important to analyse the feedstock material.

6.2 POWDER CHARACTERISATION

All the feedstock powder particles were found to have a spherical shape which is typical of agglomerated powders; a result of the spray drying and sintering process used to manufacture the powders. The powder particles were also very porous and at a high resolution the angular nature of the WC grains could be clearly observed. The WC grains were covered by the binder phase in both the WC-12%Co and the WC-10%Co-4%Cr starting materials.

University of Cape Town

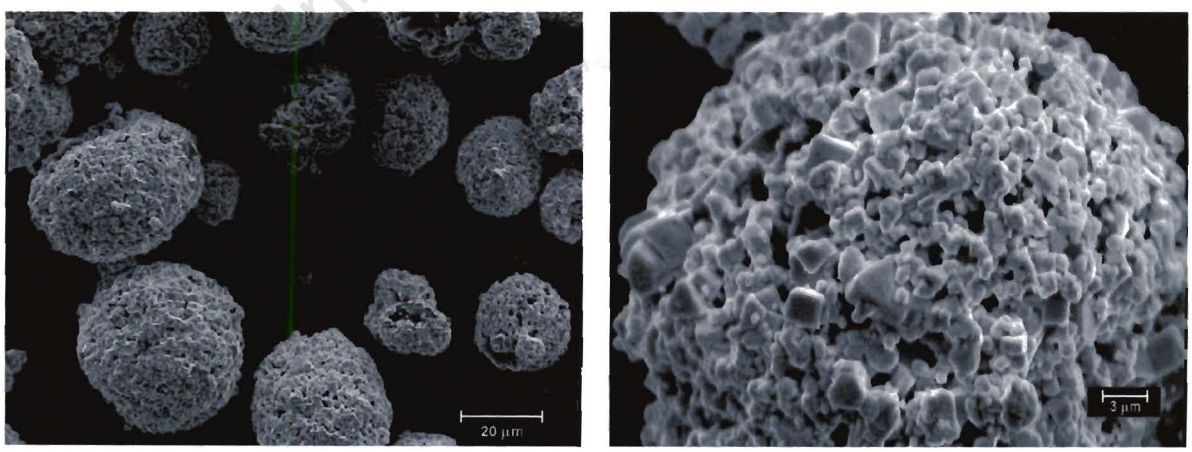

Figure 6.1: Scanning electron micrographs of the WC-12Co feedstock powder used in the spraying of the JP5000 WC-12Co HVOF Coating

The size distribution of the powder particles was determined using a Malvern laser mastersizer and the average particle size for the WC-12Co powder was found to be 34 μm. The particle size varied between 10 μm and 45 μm.

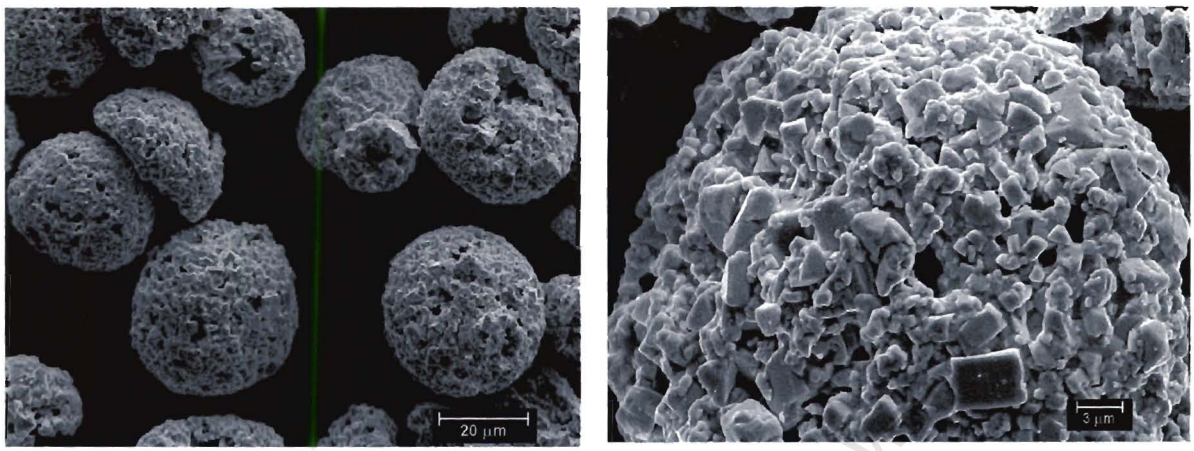

Figure 6.2: Scanning electron micrographs of the WC-10Co-4Cr feedstock powder used in the spraying of the JP5000 Wc-10Co-Cr HVOF coating

The average particle size in the WC-10Co-4Cr powder was 32 μm and this varied between 12 μm and 43 μm.

The cross sectional morphology of both powders used in this work can be seen in Figure 6.3. It is noticeable that these powders are quite porous and that the grain size of the WC grains varies widely.

An attempt was made to estimate the average WC grain size in the powders from an analysis of the cross-sectioned particle micrographs and at least fifty measurements of WC grain size were made on each agglomerated powder. The average grain size in the WC-12Co powder was found to be 1.4μm and this varied between 0.6μm and 2.6μm while the WC grain size in the WC-10Co-4Cr powder was between 0.3 μm and 1.6μm with an average of 1.1μm.

University of Cape Town

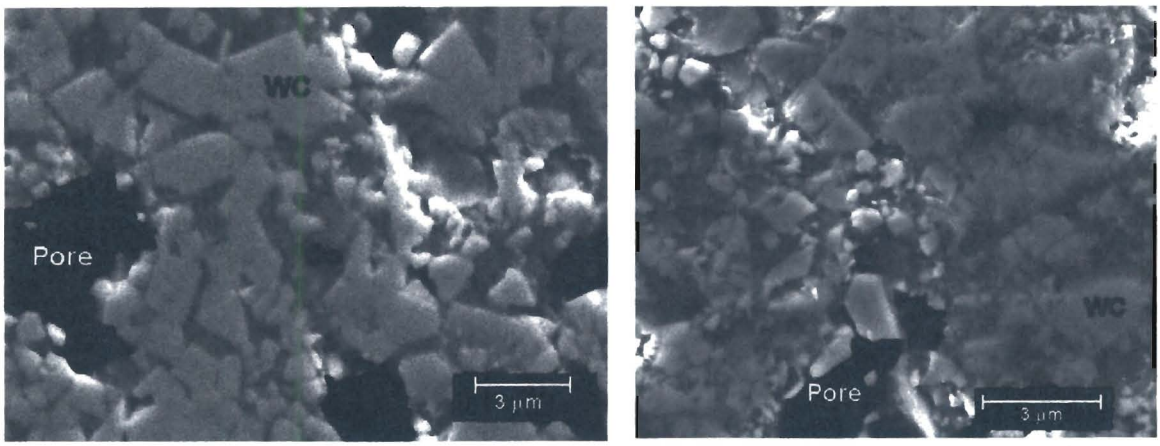

Figure 6.3: Scanning electron micrograph showing the cross-section morphology of A: a single WC-12Co powder particle and B: a single WC-10Co-4Cr powder particles

The shape of the WC grains was non-uniform with some grains having an angular morphology whilst others appeared to have a more rounded structure. However, this is probably due to the effects of the binder material coating.

6.3 Coating Microstructure

The microstructure of the four coatings was examined at low and high resolution using a scanning electron microscope. The important features that were observed were the non-homogeneity of the coatings and the wide variation in the WC grain size and shape. The coating thickness was approximately 200µm for each of the coatings but was observed to vary in thickness along the length of the substrate surface. The thinnest sections of the coating had a thickness of between 185-190µm.

Figure 6.4 shows the microstructure of the four coatings. The WC grain size varied between 0.5µm and 3.5µm in all for coatings, and the average was found to be less than 1.5µm showing a fine grain size. The level of porosity was visually estimated to be less than 10% in all the coatings, which is a characteristic of the HVOF spray process.

University of Cape Town

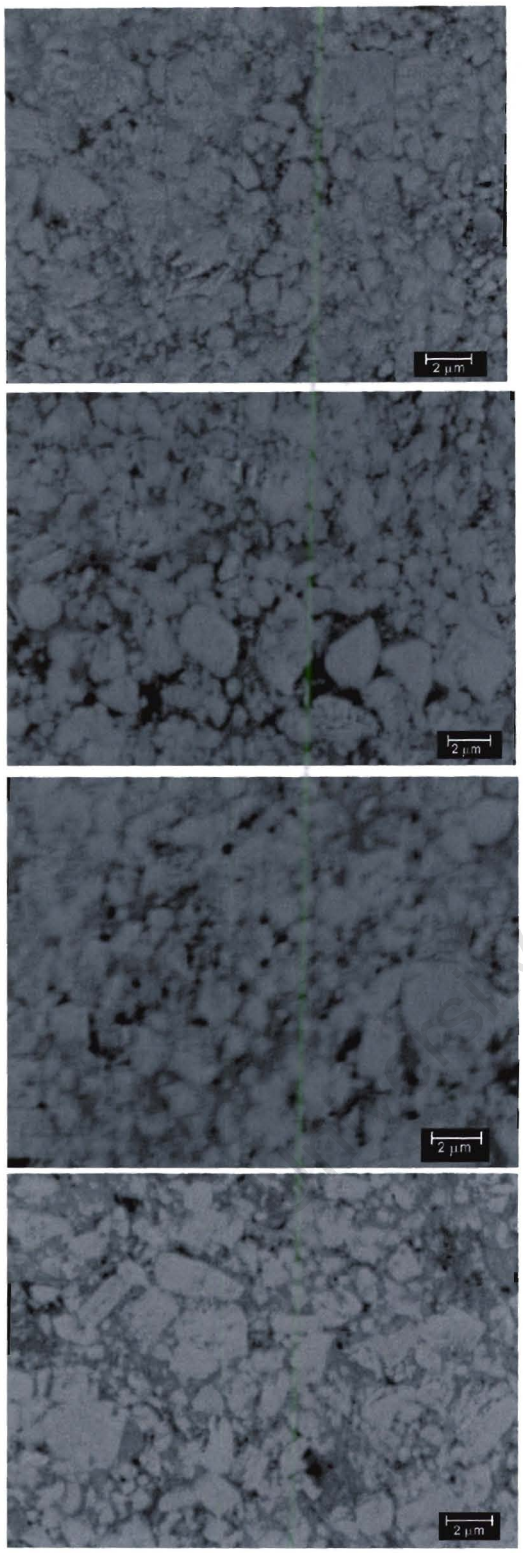

JP5000 WC-12Co coating

Grain size: 0.3-3µm

Hardness: 1159-1492HV

JP5000 WC-10Co-4Cr coating

Grain size: 0.2-2.7µm

Hardness: 1153-1431HV

DJ Std WC-10Co-4Cr coating

Grain size: 0.2-3.5µm

Hardness: 1041-1549HV

DJ New WC-10Co-4Cr coating

Grain size: 0.3-4µm

Hardness: 1264-1492HV

University of Cape Town

Figure 6.4: Scanning electron images of the four coatings The lighter regions are the WC grains and the darker grey area is the cobalt binder. The black areas indicate the areas of porosity in the coatings

It must be noted that the level of porosity is exaggerated as a result of the grinding and polishing during sample preparation which damages the coating structure.

6.4 Microstructure Of The Sintered Material

The structure and morphology of the sintered WC-12Co material was found to be more uniform compared to the coatings and the microstructure consisted of WC grains of a trapezoidal shape with sharp edges and corners. Surrounded by the cobalt binder phase. Similarly to the coatings, the WC grain size was also found to vary widely and ranged between 0.6μm and 7μm. The average WC grain size was estimated to be 3 μm.

University of Cape Town

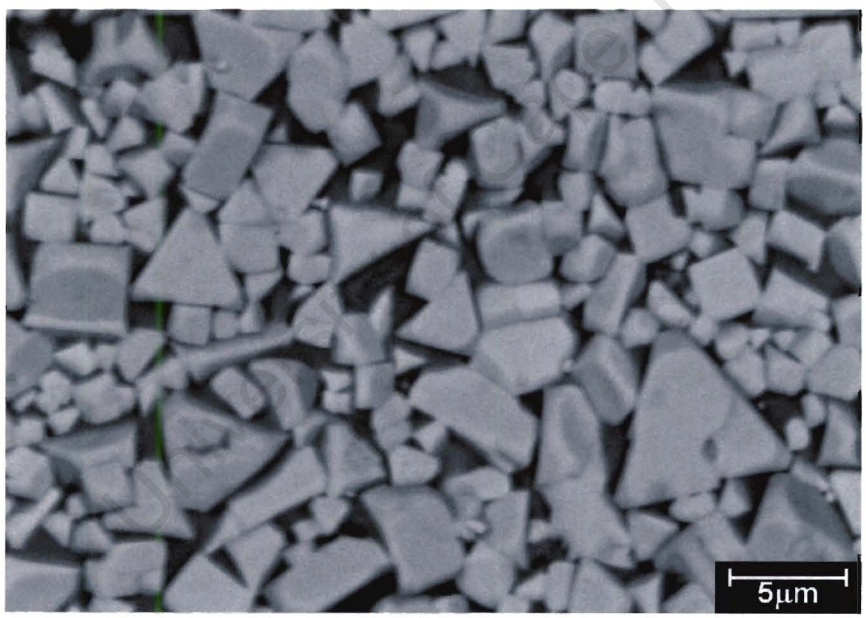

Figure 6.5: Scanning electron micrograph of the sintered WC-10Co

6.5 X-Ray Diffraction

X-ray diffraction analysis was used to determine which phases were present in the feed powders and coating materials. The XRD scans were carried out between 20° and 100° at a scan rate of $0.01°s^{-1}$.

The XRD scans of the JP5000 WC-12%Co feedstock powder and coating are shown in Figures 6.6 and 6.7. The coating was found to contain W_2C which is absent in the powder structure. This is formed by the phase transformation of the WC phase during spraying as a result of the high flame temperature.

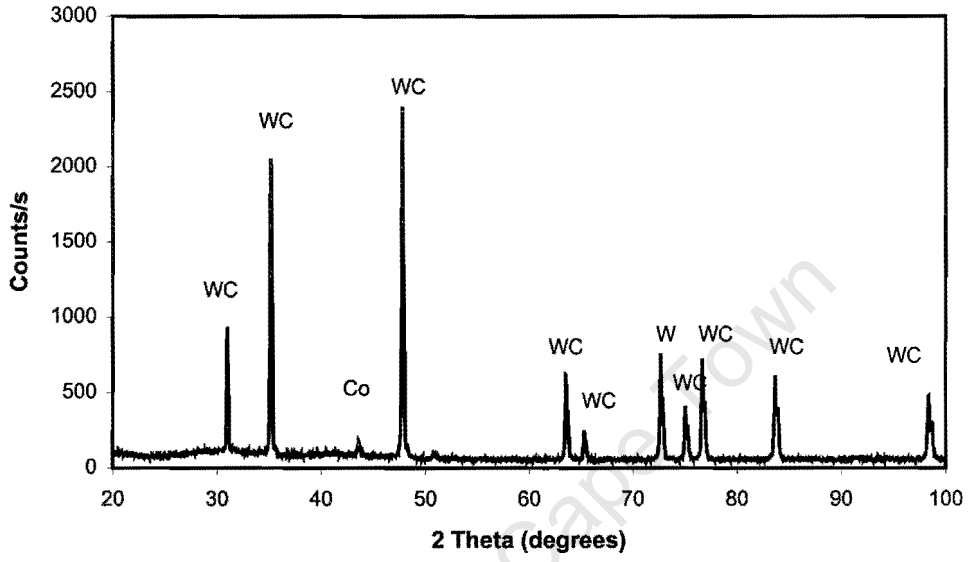

Figure 6.6: XRD scan of the JP5000 WC-12%Co feed stock powder

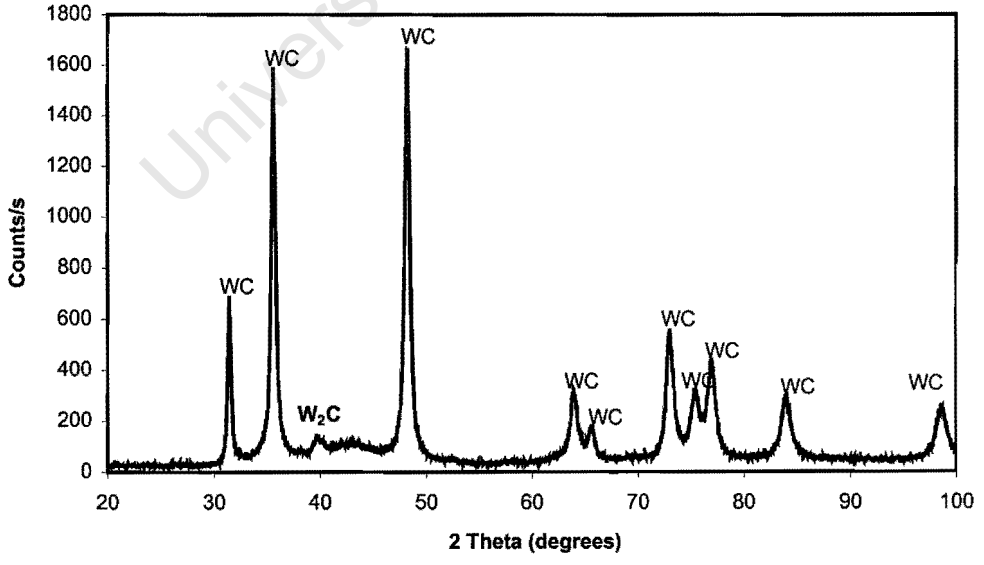

Figure 6.7: XRD scan of the JP5000 WC-12%Co coating

University of Cape Town

The XRD scan of the JP5000 WC-10%Co-4%Cr powder showed the presence of Co and W_2C, was possibly formed during agglomeration of the powder. There was no visible trace of cobalt in the coating which also contained the W_2C phase.

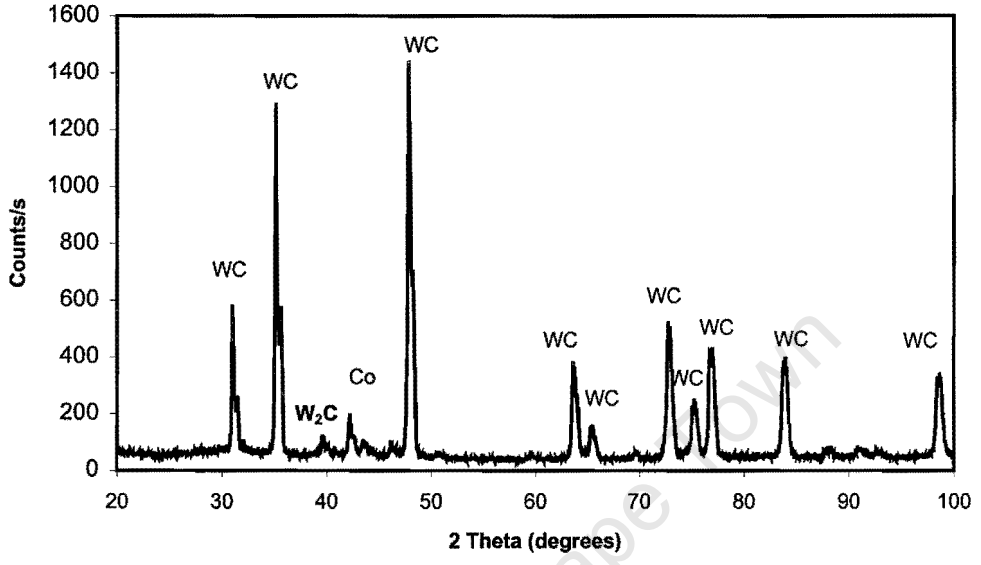

Figure 6.8: XRD scan of the JP5000 WC-10%Co-4%Cr powder

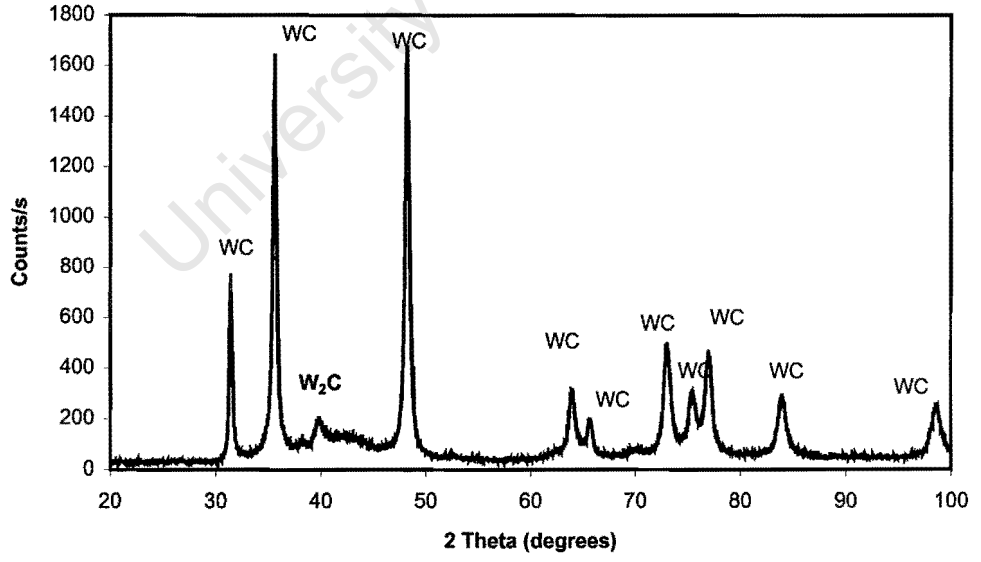

Figure 6.9: XRD scan of the JP5000 WC-10%Co-4%Cr coating

The two DJ coatings both contained the W_2C phase in addition to the Co_3W_3C which is detrimental to the wear resistance of the coatings [80].

University of Cape Town

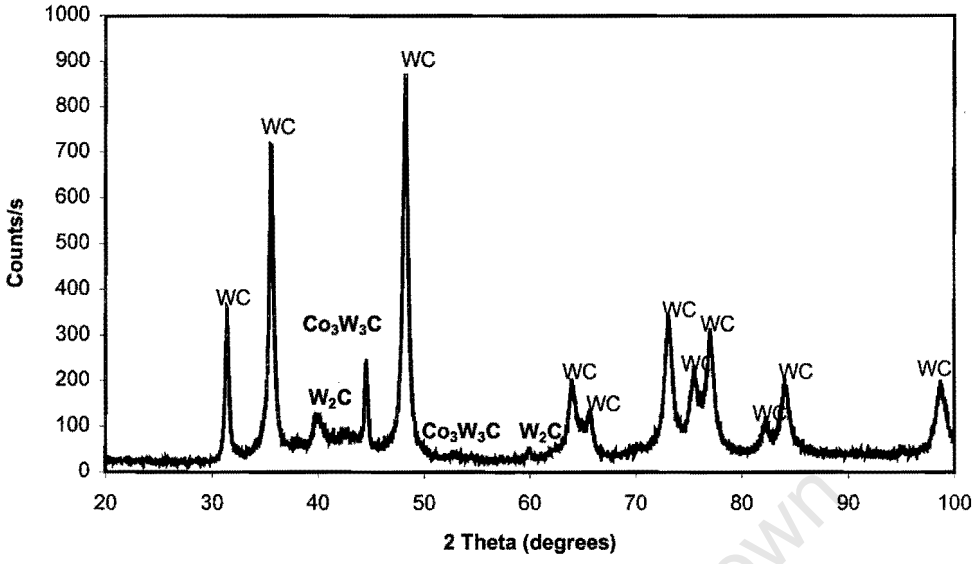

Figure 6.10: XRD scan of the DJ Std WC-10%Co-4%Cr coating

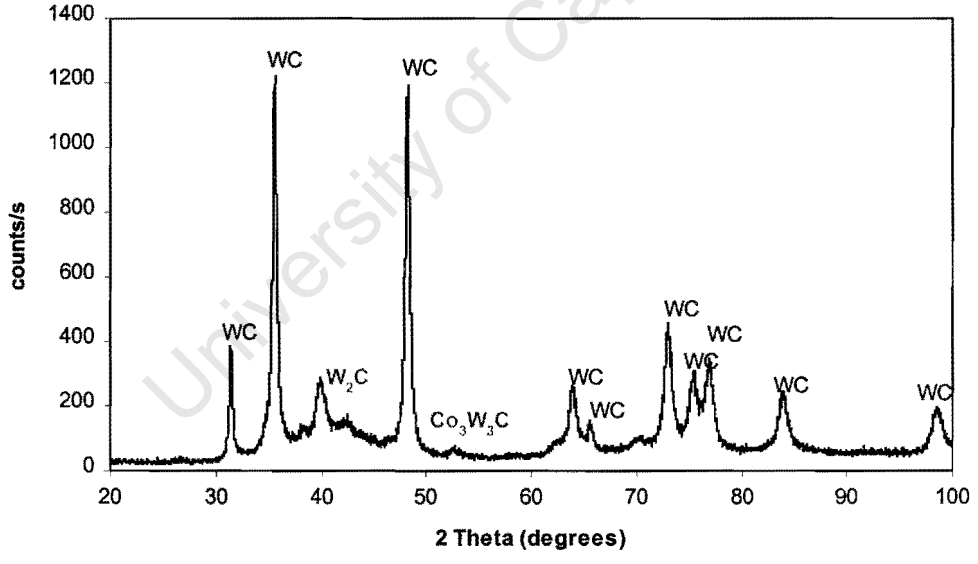

Figure 6.11: XRD scan of the DJ New WC-10%Co-4%Cr coating

University of Cape Town

6.6 MICROHARDNESS

The microhardness of each coating is shown in Table 6.1. All the coatings were shown to have hardnesses which ranged from approximately 1100HV to

1500HV. This large deviation in the recorded measurements is expected due to the nature of the coatings as shown in the previous section. The DJ New WC-10Co-4Cr coating had the highest average hardness (1383 HV) and the least standard deviation in the measurements (87). Whilst the lowest hardness of approximately 1264HV and highest standard deviation of 165 is shown by the DJ Std coating.

Table 6.1: Microhardness values of the coatings (HV 1000gf)

Coating	JP5000 WC-12Co	JP5000 WC-10Co-4Cr	DJ Std WC-10Co-4Cr	DJ New WC-10Co-4Cr
Results	1492.3	1430.8	1548.9	1492.3
	1455.0	1369.3	1455.0	1479.7
	1422.9	132.9	1438.8	1446.8
	1415.0	1347.2	1290.9	1430.8
	1407.3	1290.9	1206.7	1415.0
	1311.6	1238.1	1194.5	1407.3
	1284.2	1200.6	1182.5	1311.6
	1284.2	1194.5	1159.0	1290.9
	1251.0	1159.0	1124.9	1277.4
	1159.0	1153.2	1041.3	1264.1
Average	1348.3	1274.7	1264.3	1382.6
Std. Dev.	105.7	98.9	164.5	87.0

University of Cape Town

This large variation is thought to be primarily due to the porosity in the coatings which can result in the hardness measurements being lower than anticipated. It would seem reasonable to conclude that the 'real' hardness of the coatings are higher than the averages recorded in Table 6.1.

6.7 Dry Erosion Tests

The results of the particle erosion tests carried out on the four coatings are shown in the following sections. Testing was carried out using SiO_2 with a size range of 75-150μm and a velocity of 66ms^{-1} in the majority of tests.

Figure 6.12 shows the typical volume loss of each of the coatings as a function of the mass of erodent. It can be observed that following an incubation period the mass loss became a linear function of the amount of erodent employed. The incubation period is the result of the non-uniform coating structure, with loosely bound material on the surface being easily lost when the surface is initially impacted. The sintered material did not exhibit an incubation period indicating the uniform microstructure of the material. The wear rate was calculated from the linear portion of these graphs for each condition tested.

University of Cape Town

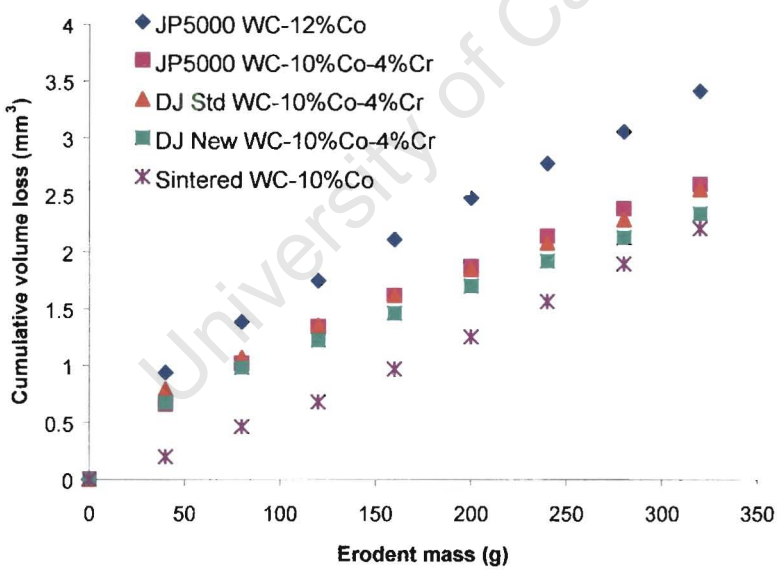

Figure 6.12: Graph showing the cumulative volume loss of the materials at an impact angle of 60° and velocity of 66ms^{-1}

6.7.1 EFFECT OF IMPACT ANGLE

In general, all the coatings showed a maximum in the wear rate at an impact angle between 55° to 60°. In the case of the WC-12Co coating, which showed the highest wear rate of all the coatings, the wear rate decreased quite sharply from its peak at 60° as the angle of impact was changed. In the case of the three WC-10Co-4Cr coatings the maximum in their wear rate curves with impact angle was much less pronounced and their overall wear rates were very similar. The maximum wear rate for the chromium containing coatings was approximately 50% less than for the WC-12Co coatings or the WC-10Co sintered material.

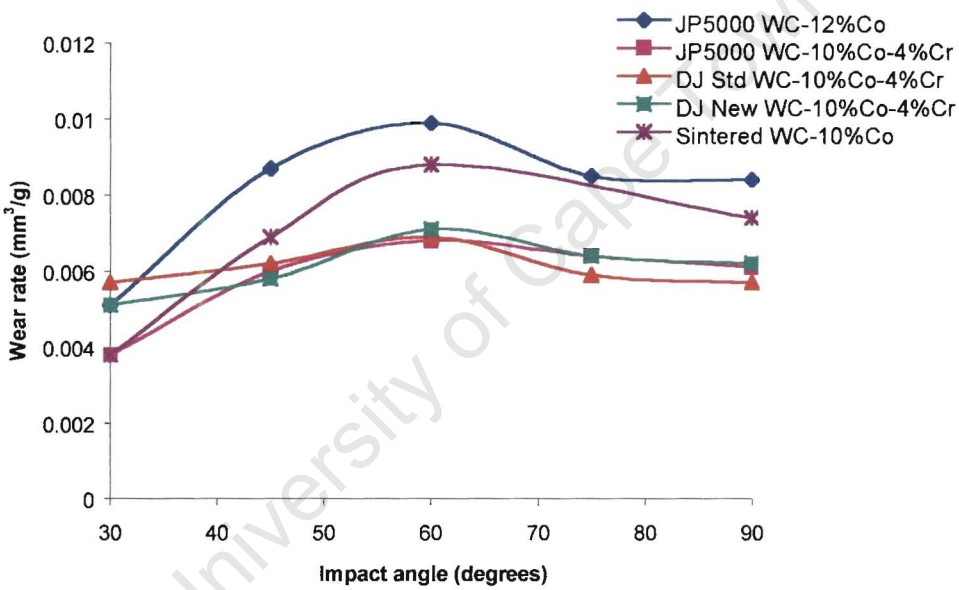

University of Cape Town

Figure 6.13: Graph showing the variation in wear rate with particle impact angle

6.7.2 EFFECT OF ERODENT PARTICLE VELOCITY

The variation in wear rate with erodent particle velocity was investigated by measuring the wear rate of the DJ New WC-10Co-4Cr coating at various erodent particle velocities between $20ms^{-1}$ and $66ms^{-1}$ using silica as the erodent material.

The relationship between the wear rate (E_R) and the erodent particle velocity (v) was found to be:

$$E_R = k\, v^n \qquad \text{Eqn. 6.1}$$

Where k is a constant and n = 1.6 for the DJ New WC-10Co-4Cr coating that was used as the target material in the tests.

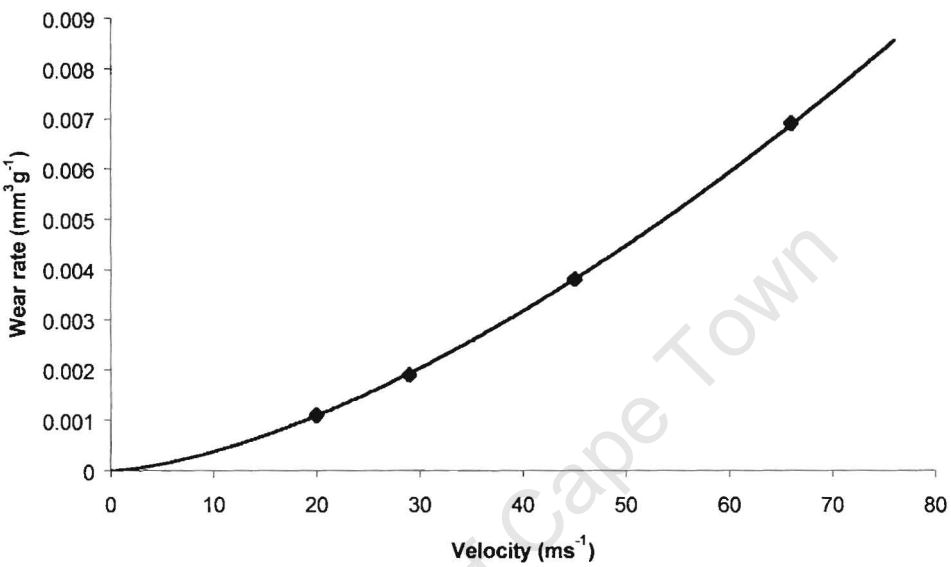

Figure 6.14: Graph showing the relationship between wear rate and erodent impact velocity for the DJ New coating

6.7.3 Effect Of Erodent Particle Size

It was difficult to get different size samples of the SiO_2 used in the majority of the wear tests but SiC was available in a wide range of particle sizes therefore it was selected as the erodent. However, SiC is much harder and more angular than SiO_2 and extrapolation of the results have to be viewed with caution.

Two different materials were employed for this work, the DJ Std coating and the sintered WC-10Co material. The tests were conducted at an impact angle of 60° and a velocity of $66ms^{-1}$. The size ranges of the SiC particles used is shown in Figure 6.15. The wear rate appeared to be independent of the erodent particle size for the DJ Std WC-10Co-4Cr coating. However the sintered WC-10Co

University of Cape Town

showed a 35% decrease in the wear rate with an increase in the SiC erodent particle size from 106μm to 710μm.

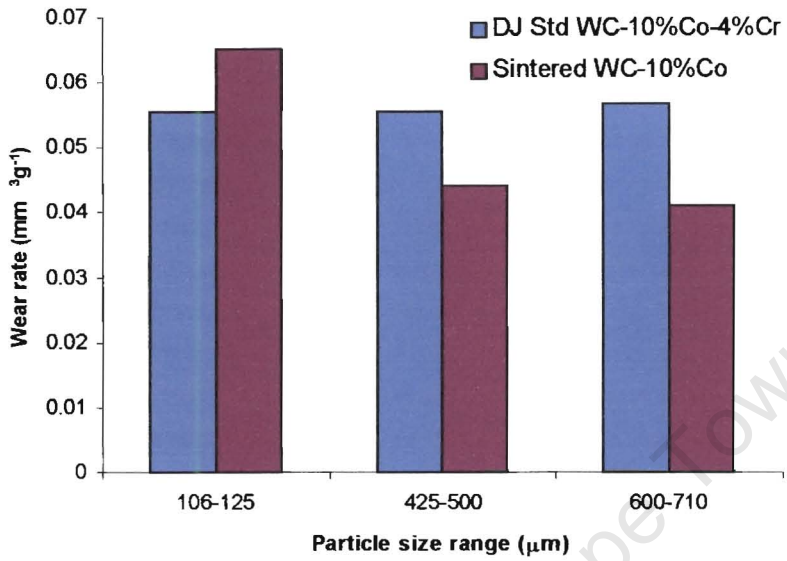

Figure 6.15: Graph showing the variation in wear rate with erodent particle size

6.7.4 Effect Of Erodent Particle Hardness

Tests were conducted at an impact angle of 60° and velocity of 66ms^{-1}. SiC and SiO_2 were used as erodents to determine the effect of particle hardness on the erosion rate. SiC has a hardness of 2500HV and SiO_2 has a much lower hardness of approximately 1200HV. Both the DJ Std WC-10Co-4Cr coating and the sintered WC-10Co material showed a significant increase in the wear rate when the erodent was changed from SiO_2 to SiC. The wear rate increased by approximately 800% for both materials. Nevertheless, the coating showed a higher wear resistance than the sintered material in both tests. Another important feature to be considered is the shape of the erodent particles. SiO_2 particles have a rounded morphology with smooth edges whereas SiC particles are angular with sharp edges and corners, as shown in Figures 5.3 and 5.4. The particle shape is known to have an effect on the wear rate and therefore the

University of Cape Town

change in wear rate is the result of the combined effect of changing particle hardness and morphology.

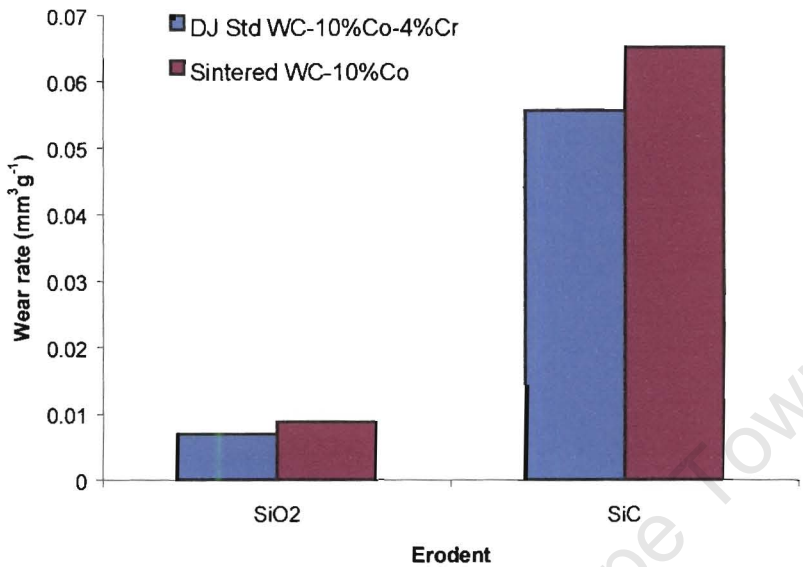

Figure 6.16: Graph showing the change in the wear rate with erodent particle hardness

6.7.5 MICROSTRUCTURE OF WORN COATINGS

The damaged surfaces of the worn coatings and sintered materials were examined using a scanning electron microscope to determine the mechanism of material loss that occurred.

Figure 6.17 shows the structure of DJ Std coating as-sprayed and after impact with SiO_2 particles at a velocity of $66ms^{-1}$. The micrograph shows a brittle mechanism of erosion characterized by the cracking and the loss of WC grains from the coating surface.

University of Cape Town

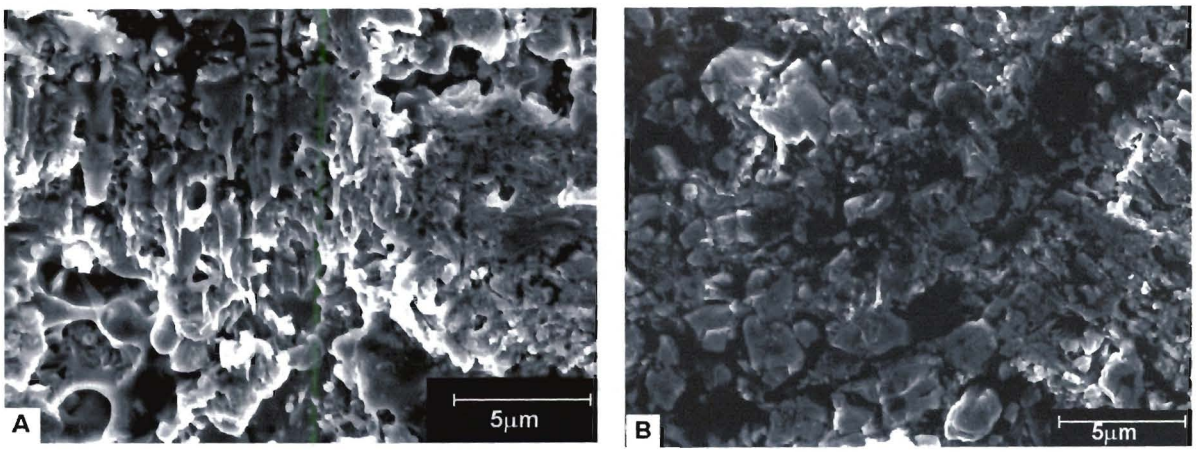

Figure 6.17: Scanning electron micrograph of the damaged surface of the DJ Std coating (a) as-sprayed and (b) after impact with SiO_2

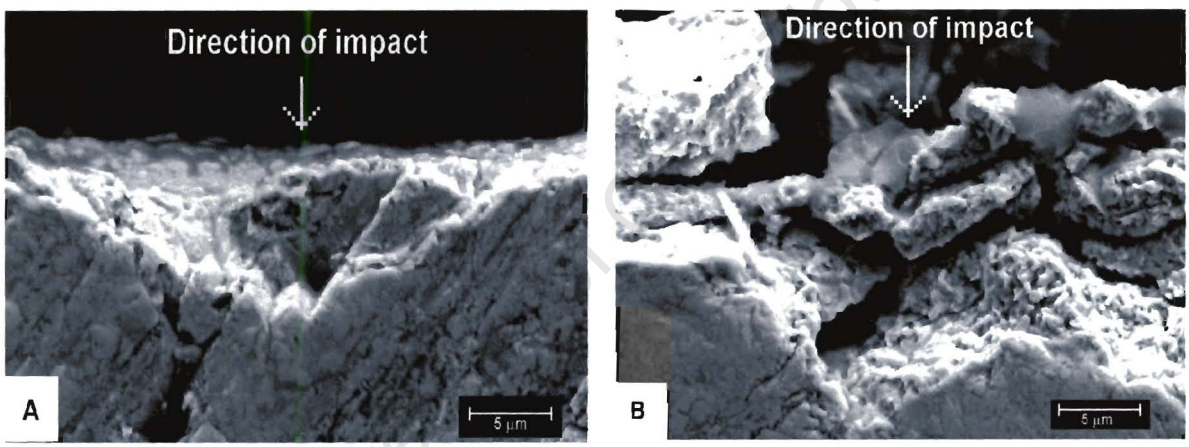

Figure 6.18: Scanning electron image of the damaged surface of the JP5000 WC-12Co coating (a) after impact with SiO_2 and (b) after impact with SiC

With silica as the erodent the damage to the coating surface was less severe as seen in Figure 6.18a, which shows the worn surface of the JP5000 WC-12Co coating after impact with SiO_2 particles at an impact angle of 60° and velocity of 66 ms^{-1}. With SiC there is more extensive cracking on the coating surface. This resulted in the loss of whole coating fragments as the cracks interlinked.

Figure 6.19 shows the damaged surface of the sintered WC-10Co material after impact with silica at an angle of 60° and velocity of 66ms^{-1}. The micrographs show binder removal and WC grain fall out. The material loss probably occurred

via a two step mechanism which involved the initial extrusion of the Co binder followed by WC grain fall out. There was also cracking of the WC grains which is shown in Figure 6.19.

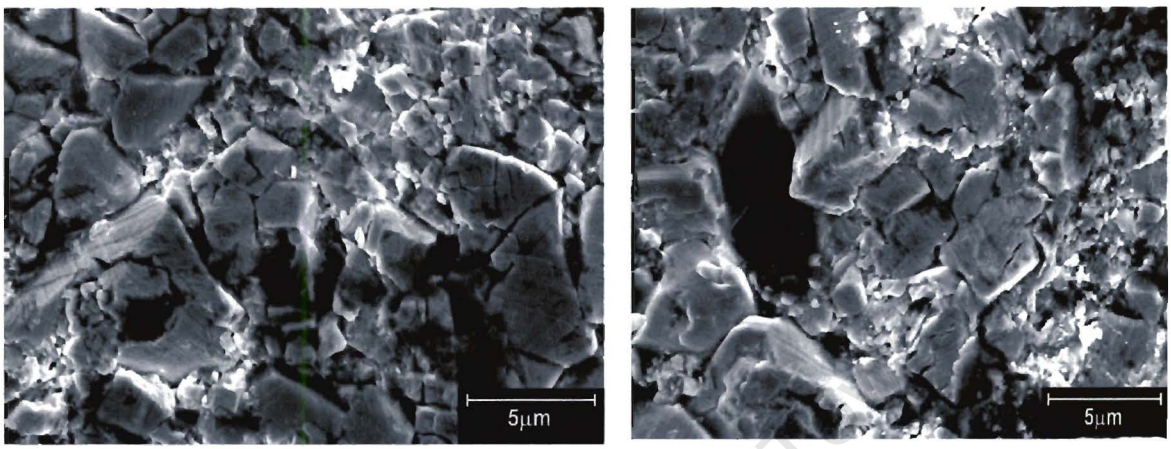

Figure 6.19: The surface of the sintered WC-10Co material after impact with SiO_2

With SiC the material loss occurred via a combination of brittle and ductile mechanisms. Figure 6.20 shows the presence of wear grooves on the worn surface of the sintered material. At higher resolution however, the fracture of WC grains can be seen in addition to binder extrusion, Figure 6.21.

University of Cape Town

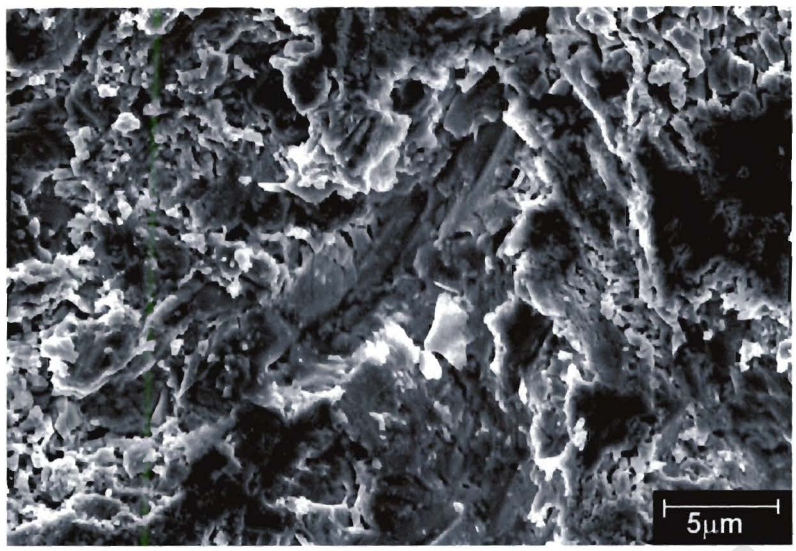

Figure 6.20: Damaged surface of the sintered WC-10Co material showing cobalt extrusion and wear grooves after impact with SiC

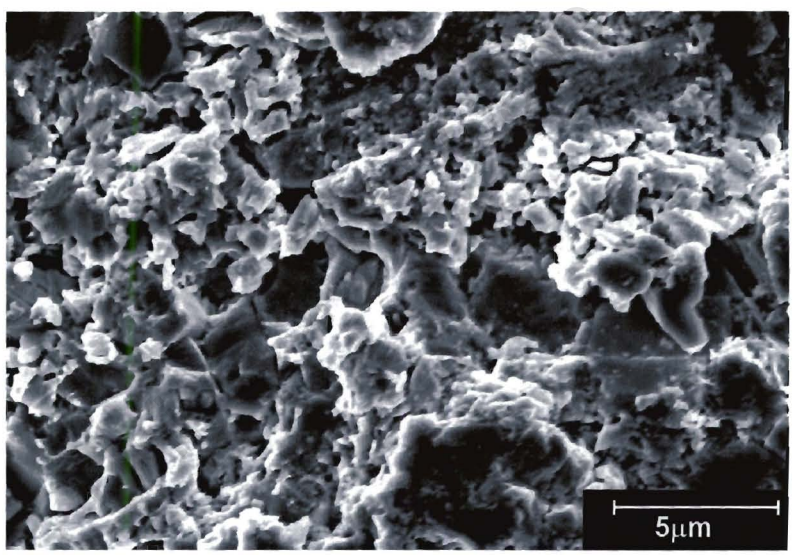

Figure 6.21: Surface of the sintered WC-10Co material after erosion with SiC particles at an impact angle of 60°

6.8 SLURRY EROSION

The results of the slurry erosion tests carried out on the four coatings are shown in the following section. The test slurry was an 11wt% SiO_2 and water slurry with a flow rate of 9 $lmin^{-1}$ giving a slurry velocity of 7ms^{-1}.

Figure 6.22 shows the typical volume loss of the coatings as a function of exposure time to the slurry. The incubation period was less pronounced than in the particle erosion tests and subsequent volume loss was a linear function of exposure to the slurry.

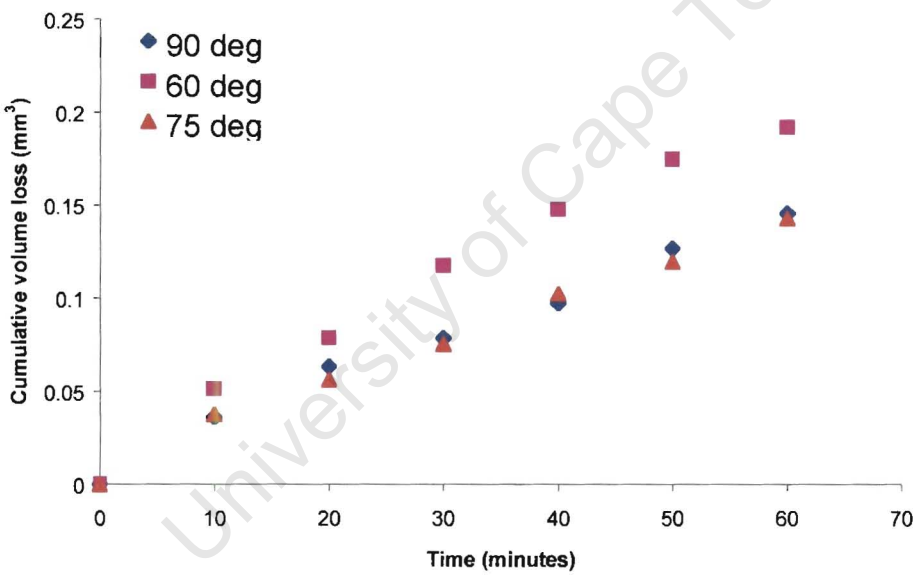

University of Cape Town

Figure 6.22: Graph showing the cumulative volume loss of the JP5000 WC-12Co coating as a function of test time

6.8.1 EFFECT OF IMPINGEMENT ANGLE

The three WC-10Co-4Cr coatings showed a maximum wear rate at 75° whereas the WC-12Co coating exhibited a maximum at 60°. The WC-12Co coating was the least wear resistant and the relationship between impact angle and wear rate

was more pronounced than for the chromium containing coatings. Nevertheless, the wear rates of the WC-10Co-4Cr coatings differed significantly at impact angles between 60° and 90°. The JP5000 coating was the most wear resistant followed by the DJ Std coating and the DJ New coating. The maximum wear rate of the JP5000 WC-12Co coating was at least 150% greater than any of the chromium containing coatings.

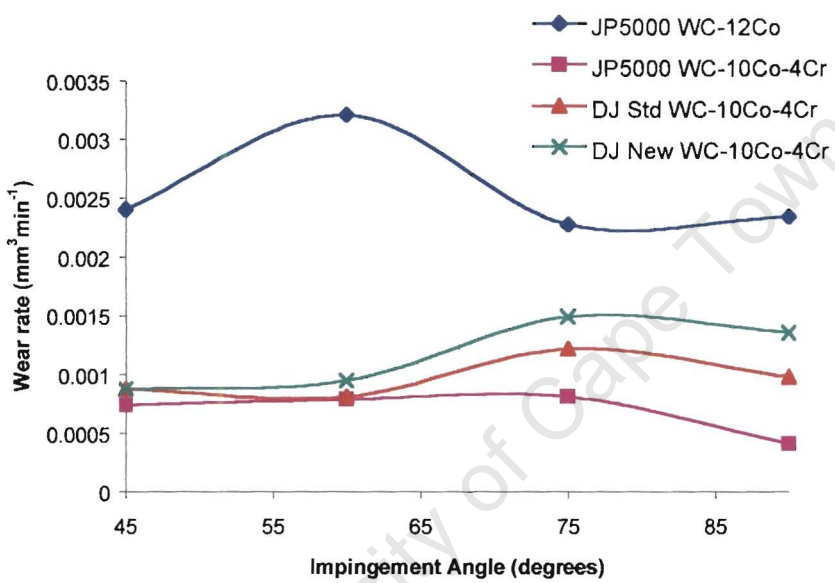

Figure 6.23: Graph showing the variation in the wear rate with slurry impact angle

University of Cape Town

6.8.2 EFFECT OF SLURRY VELOCITY

The variation in wear rate with slurry velocity was investigated by measuring the wear rate of the DJ Std WC-10Co-4Cr coating at four slurry velocities, 6.9, 5.6, 4.3 and 3.1ms^{-1}. The wear rate was found to vary with slurry velocity and an increase in velocity resulted in an increase in the wear rate of the DJ Std coating which was tested. The relationship between the wear rate (E_R) and the slurry velocity (v) was found to be:

$$E_R = k\, v^n \qquad \text{Eqn. 6.1}$$

Where k is a constant and n = 1.9.

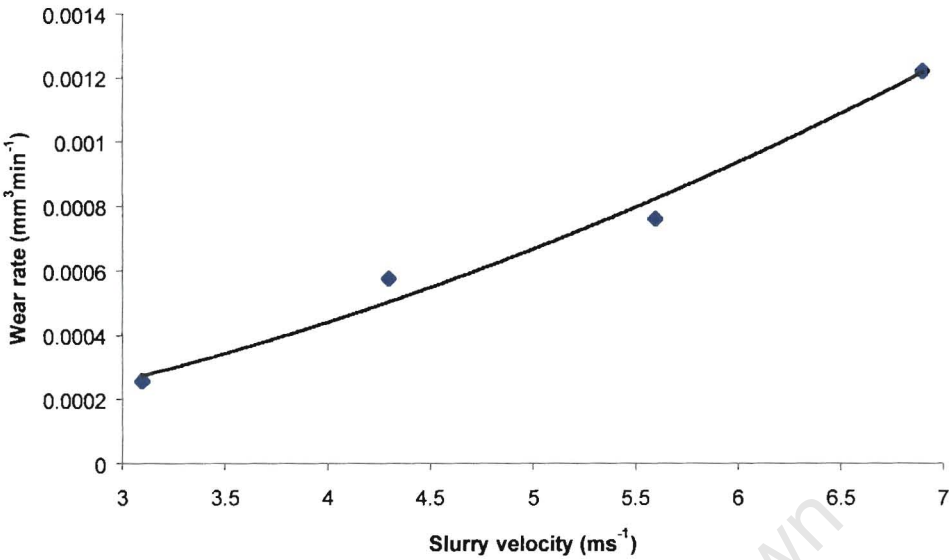

Figure 6.24: Graph showing the variation in wear rate with slurry velocity

6.8.3 MICROSTRUCTURE OF WORN COATINGS

The surfaces of the coatings were examined after exposure to the slurry to determine the mechanism of material removal that took place.

Figure 6.25 shows the worn surface of the JP5000 WC-12Co coating after testing in the slurry for 1 hour. The micrograph shows extensive cobalt extrusion, WC grain cracking and fall out.

University of Cape Town

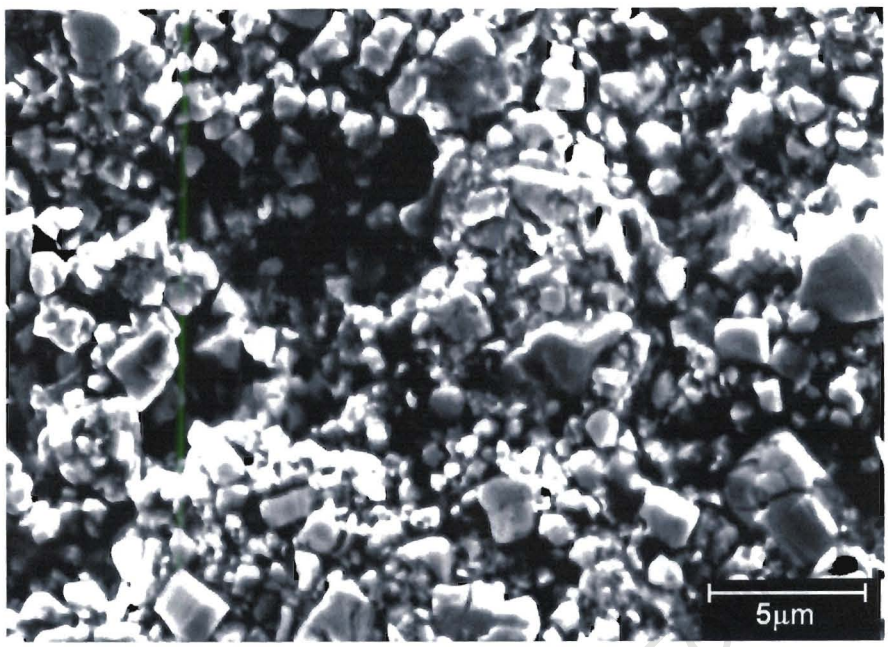

Figure 6.25: Scanning electron micrograph of the JP5000 WC-12Co after slurry testing

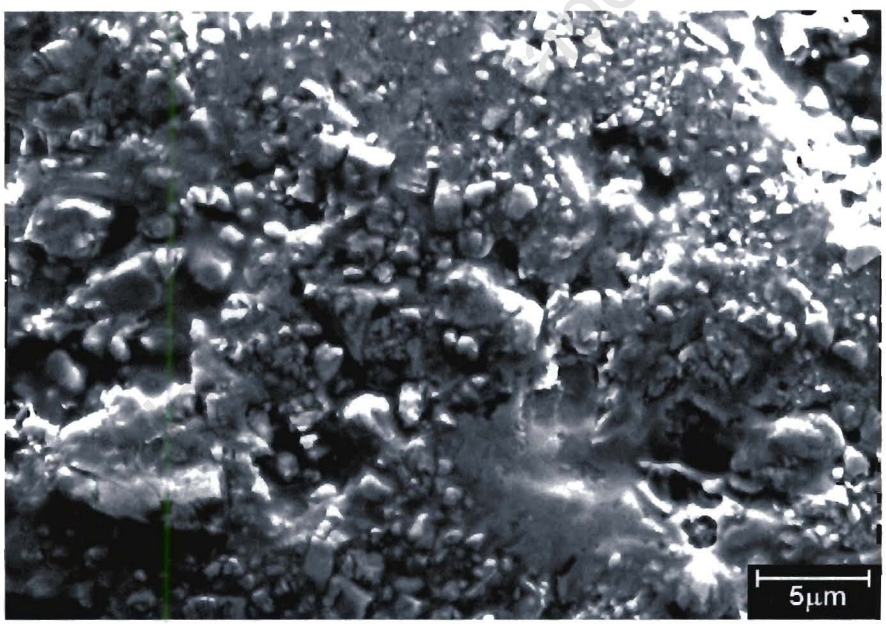

Figure 6.26: Scanning electron image of the damaged surface of the DJ New WC-10Co-4Cr coating after slurry testing

Figure 6.26 shows the worn surface of the DJ New coating after slurry testing for 1 hour. There is also evidence of binder removal. However, the extent of binder loss is less pronounced than in the WC-12Co coating. There is very little visible

binder in the damaged surface of the WC-12Co coating, whereas in the chromium containing coating, the binder phase can still be observed after exposure to the slurry for the same period of time.

6.9 Corrosion Results

Anodic polarization curves for the two coating compositions: WC-12%Co and WC-10%Co-4%Cr are shown in the Figure 6.27. As expected from the coating compositions the corrosion rate is greater for the coating containing a pure cobalt binder. In the chromium containing binder there is evidence of a small a region of passivation which occurs due to the presence of Cr.

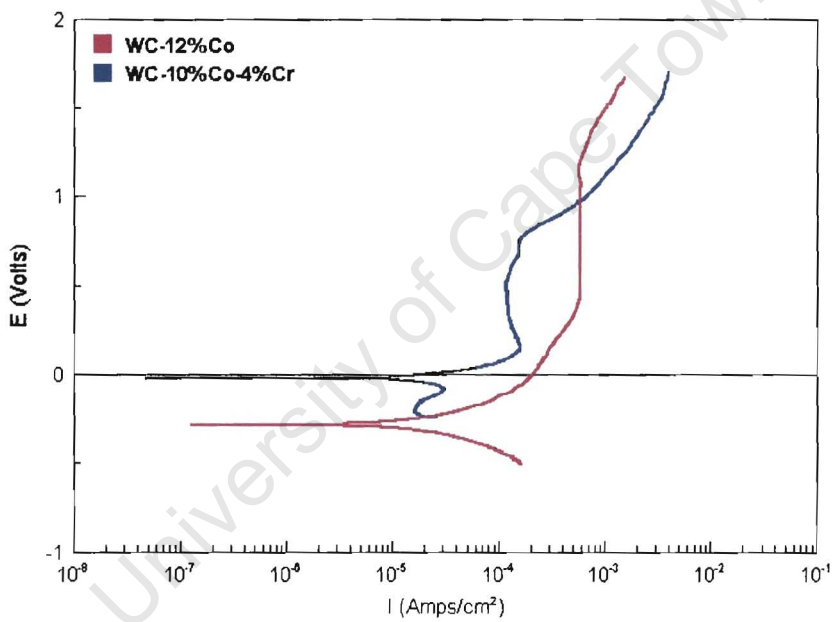

University of Cape Town

Figure 6.27: Anodic polarization curve of the WC-12%Co and a WC-10%Co-4%Cr coating in 1N H_2SO_4

Figure 6.28 shows the surfaces of the corroded coatings after testing. The micrographs clearly show the loss of binder which took place leaving a skeleton of WC grains and the presence of corrosion products on the coating surface.

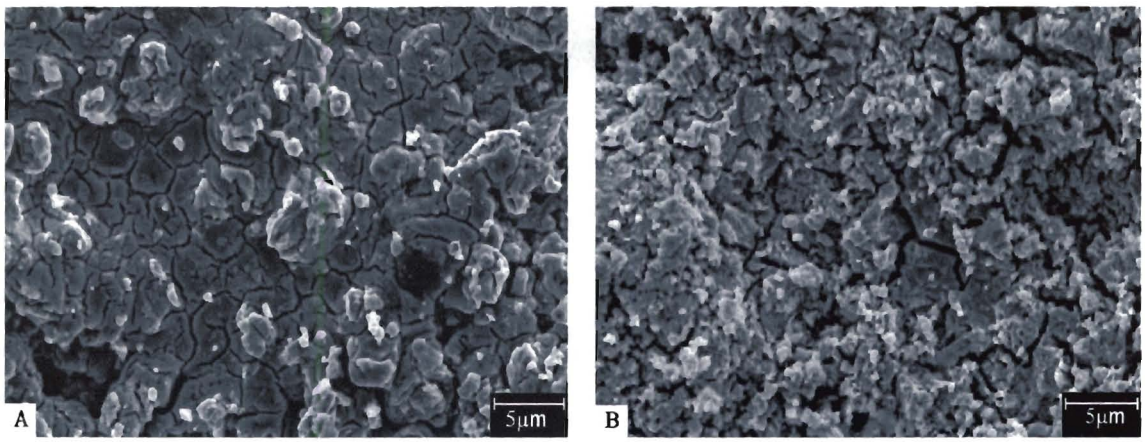

Figure 6.28: SEM micrographs of the corroded surfaces after anodic polarization in 1N H_2SO_4 (a) JP5000 WC-12%Co and (b) JP5000 WC-10%-4%Cr coatings

University of Cape Town

CHAPTER 7

DISCUSSION

7.1 INTRODUCTION

In this study the particle and slurry erosion response of a range of WC-Co(Cr) HVOF coatings has been investigated through mass loss measurements and the microscopic examination of the eroded surfaces. The coatings tested were produced using two HVOF deposition devices: the Diamond Jet system and the TAFA JP5000 system and were of two compositions: WC-12%Co and WC-10%Co-4%Cr. A sintered WC-10%Co was used as the reference material. The investigation was made to assess the relative wear behaviour of coatings produced by different systems with differing compositions.

7.2 PARTICLE EROSION

The impact angle has been shown to affect the wear rate of a material, with ductile materials exhibiting a maximum wear rate at low impact angles, usually 30° while brittle materials show a maximum wear rate at 90°. WC-Co materials are a combination of ductile and brittle phases and are therefore expected to have a maximum wear rate at angle between these two limits as was found in this work. The maximum wear rate was observed between 45° and 60° which is similar to the results of De Villiers who observed a maximum wear rate at a 60° impact angle for the coatings she studied [45].

The three WC-10%Co-4%Cr coatings showed a wear resistance that was approximately 40% better than the WC-12%Co coating, taken at their respective maximum erosion rates. Figure 7.1 shows the variation in the wear rate with impact angle of both WC-12Co and WC-10Co-4Cr produced using the same method. The reasons for this difference are difficult to ascertain since there appeared to be little difference between the structure and hardness of all the coatings as shown in section 6.2. It has been suggested that chromium improves

University of Cape Town

the cohesion between the matrix and WC grains [92]. This would clearly improve the plastic constraint in the matrix making it more difficult to deform during erosion and leading to better wear resistance. It is also believed that the increase in the mass fraction of the binder from 12% to 14% optimizes the ratio of WC to binder leading to a more efficient distribution of WC grains in the coating [92]. However this could not be confirmed in this present study.

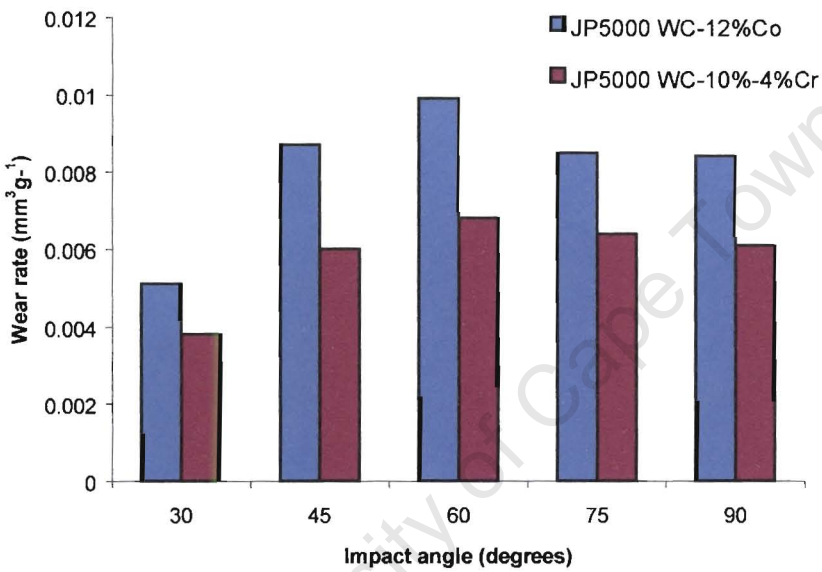

Figure 7.1: Graph showing the effect of the binder phase on the wear resistance of the JP5000 coatings

University of Cape Town

It is interesting to note that the different methods used to produce the hard metal coatings containing chromium produced coatings that exhibited very similar wear rates over the range of impact angles tested. This is clearly shown in Figure 7.2 where the variation in particle erosion rates for all impact angles is less than ±12%. The two spray methods therefore appear to have little effect on the wear resistance of the coatings. Nevertheless, the DJ New coating had a consistently lower wear resistance than the DJ Std coating.

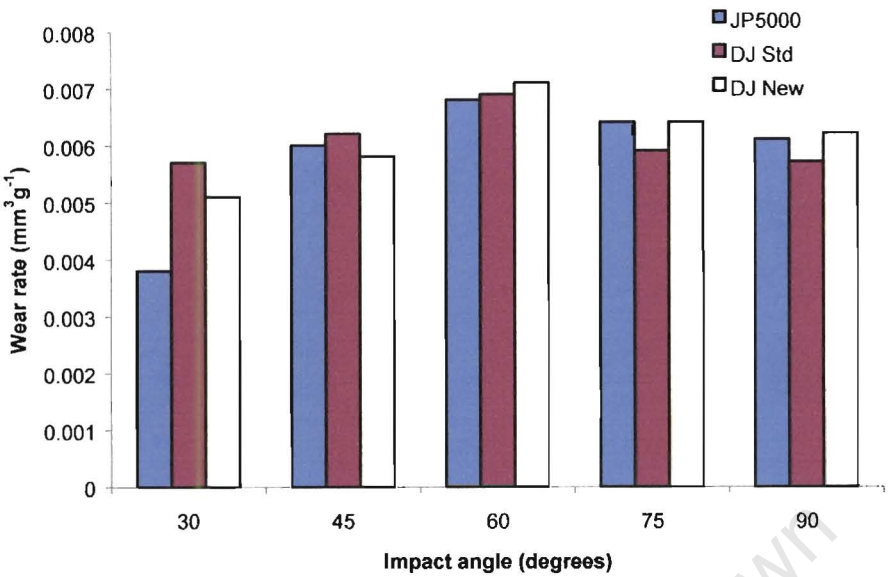

Figure 7.2: Graph showing the wear rates of the WC-10%Co-4%Cr coatings

University of Cape Town

The loss of material from the coatings was observed to occur through a variety of mechanisms. Some deformation of the matrix and cracking of the WC grains was observed but the majority of material loss occurred through cracking, chipping and spalling of the coating. This mode of removal is probably made easier by the presence of defects such as porosity, oxide stringers, regions of weak bonding between particles and the general inhomogeneity in the coating structure. Such features may assist in both crack initiation and propagation. With SiC as an erodent the damage that occurred was much more severe and the extent of crack formation and growth was observed to be more extensive with cracks penetrating the coating thickness. As a result the wear rate was found to be approximately 800% higher with SiC than with SiO_2. The hardness of SiC is 2500HV and that of SiO_2 is 1200HV, which together with the more angular nature of the particles is more effective in initiating crack formation and growth which controls the wear rate.

The wear mechanism was different for the sintered WC-10% material which exhibited two modes of material loss. The first mechanism was the extrusion of

the binder phase followed by the loss of unsupported WC grains from the damaged surface. Similar observations have been made in previous work [75, 76]. The second mode of material loss was the cracking of the WC grains which subsequently chipped causing the loss of WC grain fragments.

The effect of erodent particle velocity was shown to follow an exponential law with a velocity exponent of 1.6. This is in general agreement with work carried out by other workers who have found a velocity exponent which varies between 1.9 and 3.6 [74]. This variation in material loss with the changing particle velocity is due to the change in the kinetic energy of the impacting erodent particles. With increasing velocity, the kinetic energy ($1/2\ mv^2$) of the particles increases and there is a subsequent increase in the deformation that takes place in the target material. High impact velocities result in high energy conditions and there is rapid crack growth leading to spalling which occurs soon after the test is started. Low impact velocities produce low energy conditions and crack growth is slower and requires a greater number of particle impacts before cracks interlink and cause spalling of the coating.

The effect of erodent particle size produced very interesting results. The wear resistance of the WC-Co-Cr coating was shown to be largely independent of the erodent particle size for the range of particle sizes tested. The sintered WC-10Co material on the other hand showed a decrease in the wear rate with increasing erodent particle size. It is thought that the uniformity in the results for the sprayed coating are due to the wear behaviour being dependent on the 'toughness' of the material. Material loss, as explained earlier, is due primarily to the initiation and propagation of cracks in the coating. The ease of such events is not expected to change with changes in the size of the hard angular particles with consequent little alteration in the wear rate. The sintered material on the other hand has a more uniform microstructure. The damaged surface showed extensive deformation, extrusion of the binder and cracking of the WC grains. The larger erodent particles are less able to effectively remove Co binder from

University of Cape Town

between the WC grains since the energy is spread over a larger area, which leads to a reduction in the wear loss that occurs.

It is also interesting that the WC-Co coatings outperformed the sintered material with a similar composition. The improvement in the erosion resistance of the coatings over the sintered material can be explained by the difference in the microstructures of the two materials. The structure of the coatings is more diffuse and less well defined with a smaller grain size of 1.5μm compared to 3μm in the sintered product. The sintered material as a consequence has a lower hardness (1220HV) than the equivalent coatings [50]. These characteristics all lead to an improvement in the erosive resistance of the coatings. Such a result confirms the work of others who have found that increases in hardness and a lowering of the WC grain size lead to a better erosive wear resistance [67, 68].

7.3 SLURRY EROSION

The maximum wear rate was observed to occur at a slurry impingement angle between 60° and 75° (Fig. 6.23). Similar results were found by Wentzel and Shetty et al [50, 75].

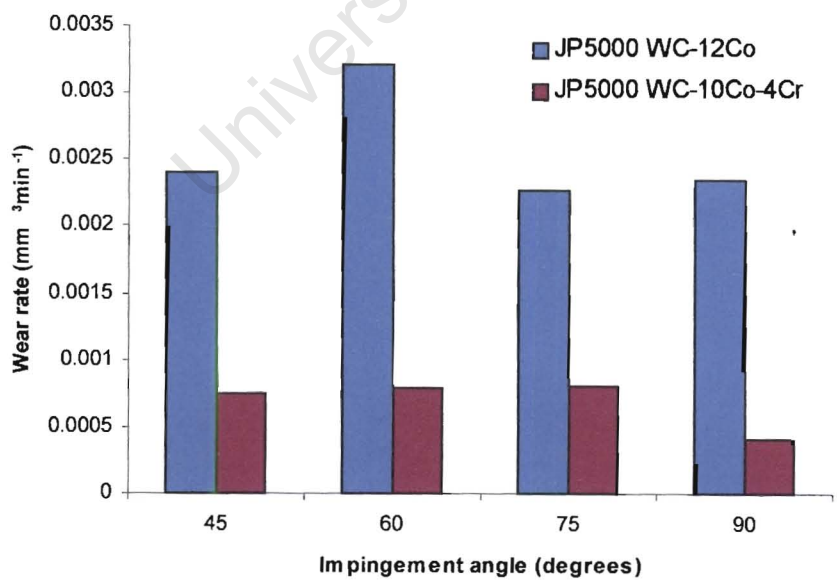

Figure 7.3: Effect of the binder phase on the slurry erosion rate

University of Cape Town

The coatings containing a 4%Cr addition outperformed the WC-12%Co coating. The maximum wear rate for the WC-12%Co coating was approximately 200% greater than those of the WC-10%Co-4%Cr coatings as shown in Fig. 7.3. The improvement in the wear resistance in the chromium containing coatings is a result of the more corrosion resistant binder. Cobalt has a lower corrosion resistance and is corroded when the coating is exposed to a corrosive medium as in the slurry test conditions. This gives rise to a strong synergistic effect on the total wear process and cobalt removal occurs through the combined effect of erosion and corrosion. The loss of cobalt undermines the WC grains which then fall out very easily. The addition of chromium, on the other hand, improves the corrosion resistance of the binder with the result that it is not removed as easily and the subsequent loss of WC grains is reduced together with the overall wear rate. Figures 7.4 shows clearly the effect of chromium addition on the degraded wear surfaces of the different coatings.

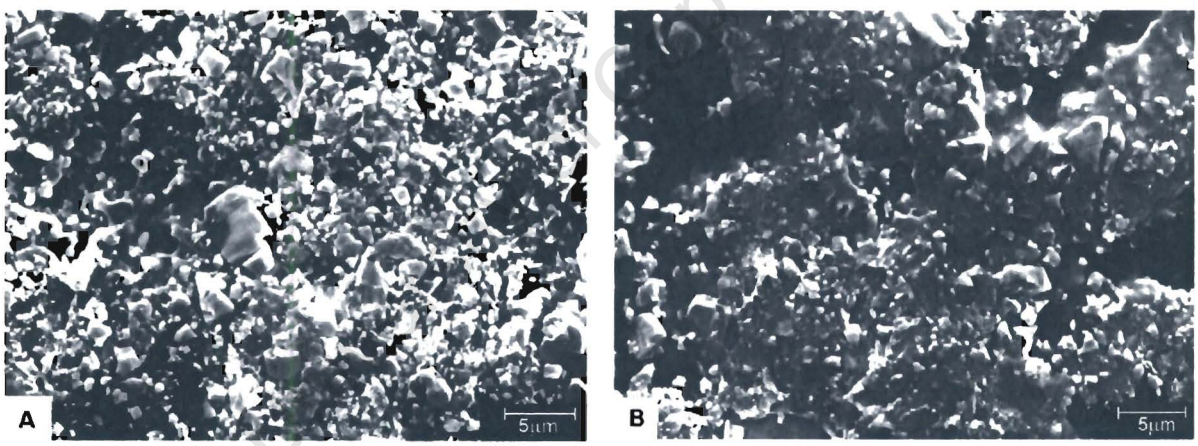

Figure 7.4: Scanning electron micrographs of (a) The worn WC-12Co coating and (b) The worn surface of the DJ New WC-10Co-4Cr coating

It should additionally be noted that the velocity of the erodent particles is very low ($7ms^{-1}$) and the particles therefore cause little deformation of the target surface resulting in a low wear rate due to erosion alone.

The poor corrosion resistance of the WC-12%Co coating when compared to the WC-10%Co-4%Cr coatings can be seen from the corrosion tests, which indicate the formation of a protective passive layer in the Cr containing coating. The higher corrosion resistance is thus a major controlling factor in the present study which agrees with the results of other workers who have found similar improvements when Cr is added to the binder phase [92, 93, 94].

The slurry wear resistance of the three WC-10%Co-4Cr coatings was found to be different with large variations in the wear rates of up to 100% between the worst and best coatings at their respective maxima. Overall the best wear resistance was shown by the JP5000 coating, followed by the DJ Std coating with the DJ New coating showing the lowest wear resistance. This could be due to the presence of the brittle Co_3W_3C phase in the DJ New coating structure as shown from the XRD scans. There could also be a greater incidence of defects in the microstructure of the DJ New coating but this could not be confirmed in the present work. This is a similar result to that found for particle erosion which suggests that the erosive wear resistance is important in slurry erosion.

University of Cape Town

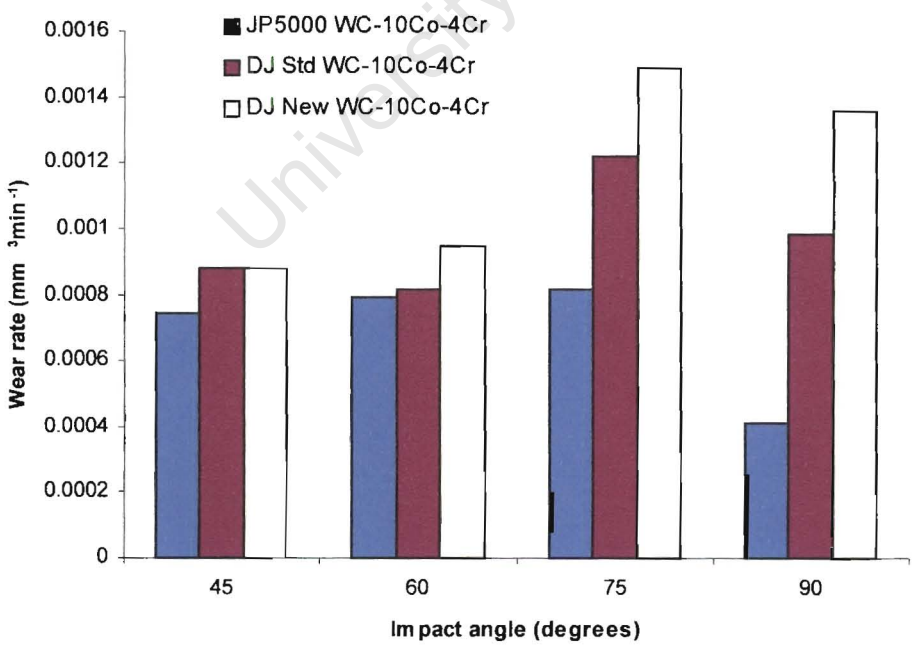

Figure 7.5: Graph showing the effect of spray method on the slurry erosion rate

The effect of slurry velocity on the erosion rate has been shown to obey an exponential law with a velocity exponent of 1.9. This is in agreement with the results of Shetty et al. who found a velocity exponent between 1.66 and 3.39 [75]. This further confirms that velocity and the erosive effect of the particles in the slurry is an important factor in the wear rate.

7.4 Comparison Of The Two Erosion Systems

A maximum erosion rate was observed between 45° and 60° in the particle erosion tests and between 60° and 75° in the slurry erosion tests. This is a result of the combination of the ductile binder matrix and the hard WC grains and the different mechanisms of material loss.

In both systems there was an improvement in the erosion resistance with the addition of Cr to the binder matrix. In the particle erosion tests the WC-10%Co-4%Cr showed a relative maximum improvement of approximately 40% whereas in the slurry tests the improvement was 200% which is considerably higher. This great improvement in the slurry erosion resistance exhibited by the Cr containing coatings is clearly due to the higher corrosion resistance of these coatings. In particle erosion the improvement is probably a result of the improved toughness of the matrix making removal more difficult.

The mechanisms of material loss in the two systems were different. In particle erosion there was extensive cracking of the coating which led to interlamellar fracture and the loss of coating fragments, whereas in slurry erosion material loss occurred mainly by the removal of the binder followed by the fall out of WC grains . There was some WC grain fracture observed in the coating surfaces after slurry erosion but this was very mild when compared with the dry particle erosion surfaces.

The effect of velocity was found to be the same for both slurry erosion and particle erosion and the erosion rates were shown to follow an exponential law with a velocity exponent which was similar in the different systems.

University of Cape Town

Whilst the addition of Cr improves the overall erosion resistance of WC-Co coatings, the level of improvement however will depend on the particular circumstances since parameters such as temperature, liquid and erodent constitution, velocity and time all play a role in the system. Any quantitative results from one system therefore have to be viewed with caution.

University of Cape Town

CHAPTER 8

CONCLUSIONS AND RECOMMENDATIONS

In this study a series of four WC-Co HVOF coatings have been subjected to both particle and slurry erosive wear. From an analysis of the results the following several conclusions may be drawn.

1. The addition of chromium to the binder matrix improves both the particle and slurry erosive resistance of the coatings. The improvement in the erosive wear resistance is more pronounced when testing was conducted in a SiO_2 slurry. The improved properties, including corrosion resistance of the Cr containing coatings is believed to be mainly responsible for this improved wear resistance.

2. The effect of impingement angle dependency is the same for the coatings in both particle and slurry erosion. The wear rates were found to reach a maximum between 45° and 75°.

3. The velocity exponent is similar, 1.6 and 1.9 for particle and slurry erosion respectively.

4. A sintered WC-10Co had a lower wear resistance than the coatings. The poorer performance of the sintered material is attributed to the larger grain size in the material.

5. The wear rate increased considerably when the erodent was changed from SiO_2 to SiC. This demonstrated that the wear rate of WC-Co materials increases with increasing erodent particle hardness and angularity.

University of Cape Town

6. The wear rate of the WC-Co-Cr coatings is independent of the erodent particle size due to the nonhomogeneous microstructure of the coating. Sintered WC-Co materials are affected by the erodent particle size with the wear rate decreasing with increasing SiC erodent particle size in the range 106-710μm.

7. There appears to be little difference between the JP5000 and DJ Std spray methods. However, the DJ New spray method appears to produce coatings with an inferior wear resistance to the other two methods. The wear resistance of the DJ New coating was the lowest in both the particle and slurry erosion tests.

RECOMMENDATIONS

The structure and influence of the coatings on the erosive wear process needs to be examined in more detail than carried out in this study since the mechanism of erosion differs to that for sintered material.

Secondly the synergistic effect between erosion and corrosion in the slurry erosion behaviour of these materials should be studied further. This could be determined by investigating the effect of increasing slurry velocity to the levels experienced during solid particle erosion. In addition, the effect of erodent particle size and hardness could also be examined since these parameters have been shown to affect the particle erosion resistance

University of Cape Town

CHAPTER 9

REFERENCES

1. K.-H. Zum Gahr, Microstructure and wear of materials, Amsterdam: New York, Elsevier, 1987.
2. E. Rabinowicz, L. A. Dunn and P. G. Russel, A study of abrasive wear under three-body conditions, Wear, **4** (1961) 345.
3. L. Fang, X. L. Kong, J. Y. Su and Q. D. Zhou, Movement patterns of abrasive particles in three-body abrasion, Wear **162-164** (1993) 782.
4. Y. Xie and B. Bushan, Effects of particle size, polishing pad and contact pressure in free abrasive polishing, Wear **200** (1996) 281.
5. K.-H. Zum Gahr, Wear by hard particles, Tribology International **31** (1998) 587
6. I.M. Hutchings, Tribology: Friction and Wear of engineering Materials, Butterworth-Heinemann, 1992.
7. V.A. Pugsley, The erosion of ultrafine WC-Co, M.Sc. Thesis, University of Cape Town, November 1998.
8. Finnie, Erosion of surfaces by Solid Particles, Wear, **3**, 1960, 87.
9. B. R. Lawn and D. B. Marshall, Indentation fracture and strength degradation in ceramics, Fracture mechanics of ceramics (Volume 3: Flaws and testing), Plenum Press, New York, 1978, 205.
10. B. R. Lawn and M. V. Swain, Microfracture beneath point indentations in brittle solids, J. of Materials Science, **10** (1975) 113.
11. I. Finnie, Some observations on the erosion of ductile metals, Wear, **19**, 1972, 81.
12. A. V. Levy and P. Chik, The effects of erodent composition and shape on the erosion of steel, Wear, **89**, 1983, 151.
13. I. Finnie, J. Wolak and Y. Kabil, J. of Mater., 2 (1967), 682.
14. I. M. Hutchings, Erosion: Prevention and Useful applications, ed. W. F Adler, ASTM, STP664, 1979, 59.
15. P. G. Shewmon, Wear, **68** (1981) 253

University of Cape Town

16. L. Brass, Effects of Microstructure of Ductile Alloys on Solid Particle Erosion, in LBL-7355, Annual Report of Materials and Molecular Research Division, Lawrence Berkeley Laboratory, 1977
17. S. Srinivasam and R. O. Scattergood, Effect of erodent hardness on erosion of brittle materials, Wear, **128**, 1988, 139
18. R. A. Vaughan and A. Ball, J. Hard Materials, 2 (3-4) (1991) 257
19. M. T. Sykes, R. O. Scattergood and J. L. Routbort, Composites, **18**, 1987, 153
20. C. T. Morrison, J. L. Routbort and R. O. Scattergood, Mater. Res. Soc. Symp Proc., 78 (1987) 207.
21. T. Foley and A. Levy, The Effect of Heat Treatment on the Erosion Behaviour of Steel, Proc. Int. Conf. On Wear of Materials, 1983, 346.
22. J. L. Routbort, R. O. Scattergood and A. P. L. Turner, Erosion of Reaction Bonded SiC, Wear , **59**, 1980, 363.
23. S. M. Wiederhorn and B. J. Hockey, Effect of material parameters on the erosion resistance of brittle materials, J. Mater. Science and Technology, **18** (1983) 766.
24. S. Wada, N. Watanabe and T. J. Tani, Ceramic Soc. Japan, ed. Yogyo-kyokai-shi, **96**, 1988, 737
25. W. J. Head, L. D. Lineback and C. R. Manning, Wear, **23**, 1973, 291
26. A. G. Evans, M. E. Gulden and M. Rosenblatt, Proc. R. Soc. London, A361 (1978) 343.
27. S. Bahadur and R. Badruddin, Erodent particle characterisation and the effect of particle size and shape on erosion, Wear, **138**, 1990, 18.
28. S. M. Wiederhorn and B. R. Lawn, J. Am. Ceram. Soc., **62** (1-2) (1979) 66.
29. A. J. Sparks and I. M. Hutchings, Wear **149** (1991) 99.
30. R. E. Winter and I. M. Hutchings, Wear **29** (1974) 181.
31. A. Misra and I. Finnie, On the size effect in abrasive and erosive wear, Wear **65** (1981) 359.
32. J. E. Goodwin, W. Sage and G. P. Tilly, J. Basic Eng., **92** (1970) 619.
33. G. P. Tilly and W. Sage, Wear **16** (1970) 447

University of Cape Town

34. J.R. Zhou and S. Bahadur, The effect of Blending of Silicon Carbide particles on the erosion of Ti-6Al-4V, Wear **132** (1989) 235.
35. A. V. Levy, Wear **68** (1981) 269.
36. R. C. Pennefather, The solid particle erosion of WC-Co Alloys, M.SC Thesis, University of Cape Town, June 1986.
37. D. Mills and J. S. Mason, Particle size effects in bend erosion, Wear **44** (1977) 311.
38. J. L. Routbort, R. O. Scattergood and E. W. Kay, Erosion of Silicon single crystals, J. Amer. Ceram. Soc.**63** (11-12) (1980) 635.
39. D.B. Marshall, A. G. Evans, M. E. Gulden, J. L. Routbort and R. O. Scattergood, Particle size distribution effects on the solid particle erosion of brittle materials, Wear **71** (1981) 363.
40. M. Bujis and J. M. Pasmans, Wear **184** (1995) 61.
41. M. E. Gulden, Erosion: Prevention and useful applications, ASTM, STP664, W. F. Adler Ed., 1979, 101
42. V. K. Sarin, Cemented carbide cutting tools, Adavances in powder technology, Ed. D. Y. Chin, ASM, 1981, 253.
43. A. A. Ogwu and T. J. Davies, Proposed selection rules for suitable binders in cemented hard metals with possible applications for improving ductility in intermetallics, J. of Mater. Science, **27** (1992) 5382.
44. Properties of sintered hardmetals customer information, Boart Longyear Research Centre, Krugersdorp, South Africa,1990.
45. H.L. de Villiers Lovelock, Effect of VC on the Microstructure and Wear resistance of WC-Co HP/HVOF Coatings, M.Sc. Thesis, University of Witwatersrand, 2000.
46. H. E. Exner, Int. Mater. Review **243** (4) (1979) 149.
47. S. E. Hankey, Cavitation erosion of WC-Co, M.Sc. Thesis, University of Cape Town, 1987.
48. D. N. French and D. A. Thomas, Hardness anisotropy and slip in WC crystals, Transactions of the AIME, **233** (1965) 950.
49. W.Schedler, Hartmetall für den Praktiker, VDI-Verlag, Düsseldorf, 1988, 5

University of Cape Town

50. V.A. Pugsley, The erosion of ultrafine WC-Co, M.Sc Thesis, Univesity of Cape Town, 1998.
51. D. C. Drucker, High strength Materials, Ed. V. F. Zackay, New York and London , John Wiley, 1965, 795
52. H. E. Exner and J. Gurland, A review of parameters influencing some mechanical properties of tungsten carbide-cobalt alloys, Powder Metallurgy. **13** (25) (1970) 13-21.
53. G. S Kreimer et al., Physics Met. Metall., **17** (1964) 85.
54. E. W. Engle, Powder Metallurgy, Ed. J. Wulff, 1942, 436.
55. J. Gurland, Trans. Met. Soc. AIME, **227** (1963) 1146
56. J. Gurland and P. Bardzil, J. Metals, Trans. AIME, February, (1995) 331.
57. G. S. Kreimer et al., Phy. Met. Metallography, **13** (6) (1962) 91.
58. J. Gurland, Trans. Metall. Soc. AIME **236** (1966) 642.
59. A. V. Laptev, Intercarbide surface is the main obstacle to increase fracture toughness and strength of hardmetals, in PM'94; Powder Metallurgy World Congress, Paris June 1994, Les Editions de Physique, Les Ulis, France, 103.
60. K. Anand and H. Conrad, Microstructure and scaling effects in the damage of WC-Co alloys by single impacts of hard particles, Journal of Materials Science **23** (1988) 2931.
61. A. A. Dankin, The resistance of some refractory compounds and hard alloys to wear induced by a high speed abrasive laden air stream, Soviet Powder Metallurgy (transl. From Poroshkovaya Metallurgiya) **94** (1970) 841.
62. A. Ball and A. W. Paterson, Microstructural design of erosion resistant hard metals, 11th Int. Plansee Seminar, Pub. Metallwerk Plansee, Reutte, Austria, **2** (1985) 377.
63. A. J. Ninham and A. V. Levy, The erosion of carbide-metal composites, Wear **121** (1988) 347.
64. M. K. Keshavan and N. Jee, Abrasion and Erosion of WC-Co Alloys, Metal Powder Report **42** (12) (1987) 181.
65. D. M. Freinkel and S. Bartolucci Luyckx, Energy loss mechanisms in the erosion of cemented tungsten carbide, Scripta Metall. **23** (1989) 659.

University of Cape Town

66. V.A. Pugsley and C. Allen, Microstructure/property relationships in the cavitation erosion of tungsten carbide-cobalt, Wear **233-235** (1999) 93.

67. K. Uuémyis, I. Kleis, V. Tumanov and T. Tiideman, Abrasive erosion of sintered tungsten carbide based hard alloys, Soviet Powder Metall. (transl. from Poroshkovaya Metallurgyia) **135** (3) (1974) 248.

68. S. F. Wayne, J. G. Baldoni and S.-T. Buljan, Abrasion and erosion of WC-Co with controlled microstructures, Tribology Trans. **33** (4) (1990) 611.

69. V.A. Pugsley and C. Allen, Microstructure/property relationships in the slurry erosion of tungsten carbide-cobalt, Wear **225-229** (1999) 1017.

70. H. Reshetnyak and J. Kuybarsepp, Mechanical properties of hard metals and their erosive wear resistance, Wear **177** (1994) 185.

71. U. Beste, L. Hammerström, H. Engqvist, S. Rimlinger and S. Jacobson, Particle erosion of cemented carbides with low Co content, Wear **250** (2001) 809.

72. Z. Feng and A. Ball, The erosion of four materials using seven erodents-towards an understanding, Wear **233-235** (1999) 674.

73. K. Anand, C. Morrison, R. O. Scattergood, H. Conrad, J. L. Routbort and R. Warren, Erosion of multiphase materials, 2nd Int. Conf. Science Hard Materials, Rhodes 1986.

74. H. Conrad, D. McCabe and G. A. Sargent, Effects of microstructure on the erosion of WC-Co alloys, Proc. Int. Conf. On the Science of Hard Materials, Jackson, Wyoming, August 1981, Pub. Plenum Press, New York, 1983, 775.

75. I. G. Wright, D. K. Shetty and A. H. Clauer, Slurry erosion of WC-Co cermets andits relationship to materials properties. Proc. 6th Int. Conf. On Erosion by liquid and Solid Impact, Cambridge, UK, ELSI VII, 1983, 63.

76. D. K. Shetty, I.G. Wright and J. T. Stropki, slurry erosion of WC-Co cermets and ceramics, ASLE Transactions **28** (1), 123.

77. E.J. Wentzel and C. Allen, The erosion-corrosion resistance of tungsten-carbide hard metals, Int. J. of Refractory & Hard Materials **15** (1997) 81.

78. R. Westergård, N. Axen, U. Wiklund and S. Hogmark, An evaluation of plasma sprayed ceramic coatings by erosion abrasion and bend testing. Wear **246** (2000) 12.

University of Cape Town

79. R. C. Tucker, Plasma and detonation-gun deposition techniques and coating properties, in: R. F. Bunsah et al (eds), Deposition Technologies for Films and Coatings, Developments and Applications, Noyes Publications, NJ, 1982.
80. A.C. Bozzi and J.D. Biasoli de Mello, Wear resistance and wear mechanisms of WC-12%Co thermal sprayed coatings in three-body abrasion, Wear **233-235** (1999) 575.
81. J. Nerz, B. Kushner and A. Rotolico, Microstructural evaluation of tunsgten carbide-cobalt coatings, Journal of Thermal Spray Technology **1** (1992) 155.
82. T.P. Slavin and J.Nerz, Materials characteristics and performance of WC-Co wear resistance coatings, in: T.F. Bernecki (Ed), Thermal Spray Research and Applications, ASM International, Metals Park, OH, 1990, 873.
83. V. Ramnath and N. Jayaraman, Characterisation and Wear Performance of Plasma Sprayed WC-Co Coatings, Mater. Sci. Technol. , **5**, (1987) 382.
84. K. Korpiola and P. Vuoristo, Effect of HVOF gas velocity and fuel to oxygen ration on the wear properties of tungsten carbide coating, Thermal Spray: Practical solutions for engineering problems, Ed. C. C. Berndt, ASM International Materials Park, OH-USA, 1996, 177.
85. R. J. K. Wood, B. G. Mellor and M. L. Binfield, Sand erosion performance of detonation gun applied tungsten carbide/cobalt-chromium coatings, Wear **211** (1997) 70.
86. H. Kreye, D. Fandrich, H.-H. Muller and G. Reiners, in Proceedings of the 11th Int. Thermal Spraying Conf. , Montreal, September 1986, Canada Welding Institute, 121.
87. C. Li, a. Ohmori and Y. Harada, Effect of powder structure on the structure of thermally sprayed WC-Co coatings, Journal of Material Science **31** (1996) 785.
88. S.F. Wayne and S. Sampath, Structure/propertuy relationships in sintered and thermally sprayed WC/Co, J. Thermal Spray Technology **1**(4) (1992) 304.
89. B. G. Mellor and E. Lopez, Fracture toughness measurements on sprayed WC-Co coatings, Second Engineering Materials Post Graduate Conf., University of Southampton, UK, 1996.

University of Cape Town

90. A. Karimi, Ch. Verdon, J.L. Martin and R.K. Schmid, Slurry erosion behaviour of thermally sprayed WC-M coatings, Wear **186-187** (1995) 480.
91. C. Verdon, A. Karimi and J.-L. Martin, Microstructural and analytical study of thermally sprayed WC-Co coatings in connection with their wear resistance, Materials Science and Engineering **A234-236** (1997) 731.
92. H. M. Hawthorne, B. Arsenault, J. P. Immarigeon, J. G. Legoux and V. R. Parameswaran, Comparison of slurry and dry erosion behaviour of some HVOF thermal sprayed coatings, Wear **225-229** (1999) 825.
93. D. Toma, W. Brandl and G. Marginean, Wear and corrosion behaviour of thermally sprayed cermet coatings, Surface and Coatings Technology **138** (2001) 149.
94. M. Bjordal, E. Bardal, T. Rogne and T.G. Eggen, Erosion and corrosion properties of WC coatings and duplex steel in sand-containing synthetic sea water, Wear **186-187** (1995) 508.
95. J Berget, E. Bardal and T. Rogne,. Influence of WC Particle size and Matrix Composition on the behaviour of WC-Co-Cr Coatings sprayed by the HVOF process, Thermal Spray: A united forum for scientific and technological advances, C.C. Berndt (Ed) 1997.
96. H.L. de Villiers Lovelock and P. Van Wyk, Effect of powder type and composition on the erosion and abrasion of HP/HVOF deposited WC-Co coatings, J. of Thermal Spray Technology, **7** (3) (1998), 357.
97. J Berget, E. Bardal and T. Rogne, Effects of powder composition on the erosion, corrosion and erosion-corrosion properties of HVOF sprayed WC based coatings, Proceedings of the 15th International Thermal Spray Conference, 25-29 May 1998, Nice, France.
98. Y. Fukuda, H. Yamasa, M. Kumonn and H. Kimura, in Proceedings of the Int. Symposium on Advanced Thermal Spraying Technology and Allied Coatings, Osaka, May 12-15 1988, Japan High Temperature Society, Japan, 49.
99. Y. Wang and P. Kettunen, The Optimisation of spraying parameters for WC-coatings by plasma and detonation-gun spraying,Thermal Spray International Advances in Coatings Technology, ASM International, Metals Park, OH, 1992, 575.

University of Cape Town

100. A. W. Ruff and L. K. Ives, Measurement of solid particle velocity in erosive wear, Wear **35** (1975) 915.

101. J. Zu, I.M. Hutchings and G.T. Burstein, Design of a slurry erosion test rig, Wear **140** (1990) 331.

University of Cape Town